Bachelor's Thesis

Time evolution of the size distribution of droplets on a string

Zeitentwicklung der Größenverteilung von Tropfen auf einem Faden

prepared by

Gunnar Klös

from Vechta

at the Max Planck Institute for Dynamics and Self-Organization

Abstract

We analyze the size distribution for a system of three dimensional droplets on a one dimensional substrate and its dynamical evolution. This is done by the means of scaling theory which allows an almost exclusive use of dimensionless units. The droplets micro-dynamics are varied as well as the dimension of the volume flux onto the substrate. We then compare the resulting influences on the systems main observables: the porosity, the number of droplets and the droplet size distribution. Hence a connection between the micro-dynamics and the growth of the smallest droplets is developed.

Contents

Contents

Nomenclature

Variable	Meaning
δ	Threshold value for merging with both neighbouring droplets.
ϵ	Scaling exponent attained by fractal packing ansatz.
γ	Surface tension.
I	Interaction range of a droplet.
λ	Proportionality factor for radii dependent interaction range.
$L, l(\tau)$	Relative amount of covered substrate [per unit length].
μ	Weighting of the strings surface.
$n(s, S)$	Droplet size distribution.
$N, n(\tau)$	Number of droplets [per unit length].
$P, p(\tau)$	Relative amount of free substrate [per unit length].
ρ	Thickness of the string.
σ	Effective droplet size regarding the flux dimensionality (general case for L).
θ	Scaling exponent attained by classical scaling theory.
τ	Dimensionless time.

Nomenclature

Variable	Meaning
V	Total volume of all droplets.

1. Introduction

1.1. Breath figures

The condensation of water vapor on surfaces in form of droplets is a phenomenon we encounter on a daily basis. Examples are various and widespread: The condensation of vapor on the lid of a pan, the formation of dew on leaves (figure 1.1) or on spiderwebs (figure 1.2). The first scientific descriptions of the droplet distributions formed by breathing onto a cold glass plate, originally used to determine the cleanliness of the glass, established the term *breath figure* for this phenomenon [1].

Also in industry the condensation of vapor is a recent field of interest. For instance it is applied for humidifiers or heat exchangers, where high heat transfer coefficients are achieved by condensation [2]. In these cases it is desirable to maximize the wetted surface. In contrast, there are also fields of application where one wants to achieve the opposite: a reduction of covered area, if condensation is inevitable. An example are greenhouses, where the condensation on the windows leads to reduced light transmission [3].

Figure 1.1.: Breath Figures in nature: Dew droplets on a leaf.
source: *Jon Sullivan, CC BY-SA-3.0*

Furthermore, the creation of breath figures also finds an important application in the so called *fog harvesting*. It is used in arid regions to collect drinking water out of foggy air. For that purpose, a finely woven net is spanned vertically at some height above the ground so that the wind can blow through its meshes. That way a large amount of droplets in the air is deposited on the ribbon (theoretically 75 to 95 %, experimentally up to 66 %). Those droplets coalesce until they are big enough to drip off or slip down into some collection tank [4, 5]. The main difference of those two effects is the type of the flux: For the deposition by airflow the flux is nearly homogeneous onto the surface of the substrate. Condensation, on the other hand, is rather homogeneous onto the surface of the whole system, which additionally takes into account the surface of the already present droplets. Therefore one question

of this work is: What effects do those different kinds of fluxes have on the size distribution of droplets growing on one dimensional substrates.

Figure 1.2.: Breath Figures in nature: Dew droplets on a spider web.
source: *USFWS Photo, CC BY-SA-3.0*

Typically breath figures evolve to a vastly polydisperse distribution of droplet sizes in which self-similarity can be observed. The shape of the breath figures droplet size distribution and also the behaviour of the droplets themselves is determined by a variety of external and internal influences, such as the wetting properties of the substrate, the saturation of the environment or the van-der-Vaals forces between the molecules of the (condensed) liquid. After all, there are multiple phenomena observed in the evolution of the droplets: Besides the condensation/deposition they can evaporate again, coalesce with other droplets or be deformed because of the surface or gravity.

The main growth-processes of droplets in breath figures have been analyzed in the 1980s [6, 7]. In contrast, the microscopic processes and droplet interactions are still not completely understood.

1.2. Experimental setups

There is a wide range of every day phenomena giving an idea of the basic features needed to design an experiment to analyze three dimensional droplets on a surface of arbitrary dimension. For example, think of the lid of a cooking pan or a spiderweb covered with dew.

1. There has to be a supersaturated system tending to a phase-separation because of some gradient of temperature, concentration or similar.

2. The temperature or concentration gradient has to point in the direction of some structure of the desired dimensionality, for example, a string when considering a one dimensional surface or a glass plate for a two dimensional one.

3. The condensation on the substrate should not involve a substantial decline of this gradient.

For a specific experiment where water vapor is supersaturated in air and shall condensate on a substrate this implies a basic condition: The structure has to be cooler than its environment and has to be maintained as such or else it must be extremely hydrophilic with roughness or surface heterogeneities providing sufficient pinning of three phase contact lines to prevent the creation of a wetting film.

1.2.1. Droplets on a plate
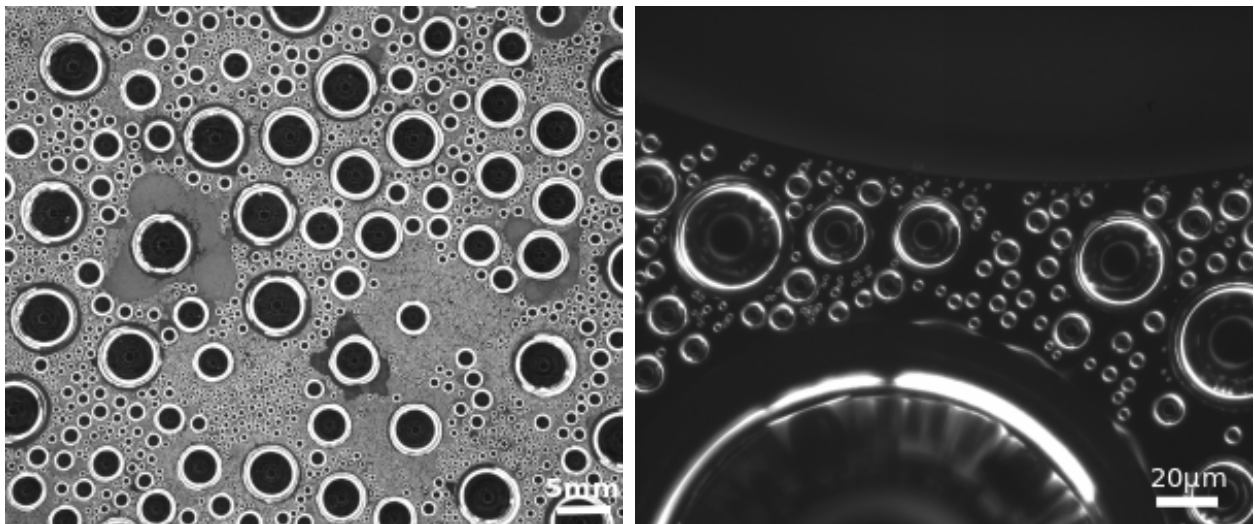
(a) Coarse resolution.   **(b)** Fine resolution.

Figure 1.3.: Water condensing in form of droplets on a polyethylene film shown in [8].

In the past various experiments on breath figures, three dimensional droplets on two dimensional substrates, has been carried out. The two panels shown in figure 1.3 are taken from an experiment performed by Tobias Lapp [8]. He heated a small amount of water at

1. Introduction

the bottom of a closed cell to produce a constant saturation level. The upper end of the cell was closed by a glass plate which was kept at a constant, much lower temperature causing the vapor to condensate on it. More precisely, the vapor was not condensing directly on the glass plate but on cling foil which provides an easy way for getting a clean hydrophobic surface.

With this experiment and additional simulations by J. Blaschke [9], the group of J. Vollmer was able to point out an interesting relation between the growth of the droplets and their size distribution.

1. They confirmed that the typical radius R grows linearly in time as shown by Family and Meakin [10].

2. They were also able to show that the size distribution of droplets follows a power law which is rescaleable for different time steps by the typical droplet size $S(t)$.

3. They determined a coalescence kernel and showed that...

   a) this kernel does not not factorize.

   b) the radius distribution is independent of the contact angle, at least for spherical caps.

   c) the exponent z' describing the asymptotic behaviour of the porosity, predicted to have a value of $z'_{\text{th.}} = 0.25$ by Blackman and Brochard [11] does not fit to the values Blaschke et al. measured in their numerical simulations ($z'_{\text{num.}} = 0.30$) and experimental data ($z'_{\text{exp.}} = 0.16$). One of the main reasons for this disagreement, is the incorrect assumption of a factorizing coalescence kernel used by [11].

   d) the results for the scaling exponent of the porosity and the size distribution of the smallest droplets in the system are not completely tractable by theory. Porosity is the expression for the not wetted area of the substrate.

4. They presented a theory for the lower cut-off of the droplet size distribution which provides qualitative predictions for the data. Since this cut-off is related to the growth rate of the smallest droplets this gives rise to a more profound analysis of the dynamics of those droplets.

For a more detailed exposition of the results mentioned in this section see [8] and [9].

So far very little numerical and experimental work specifically addressing one dimensional substrates was carried out. Besides the growing importance of breath figures in general, the one dimensional breath figures provide an easy tractable system. Especially for numerical simulations the one dimensional system offers the possibility for much faster algorithms. It also is the only other arrangement included by Blackman and Brochard that can be observed in an experiment. Therefore this work will address a numerical model of droplets growing on a string.

4

1.2.2. Droplets on a string

Parallel to the simulations underlying this work, an experiment was designed to produce comparative experimental data for the the size distributions and growth processes of droplets condensing on a string.
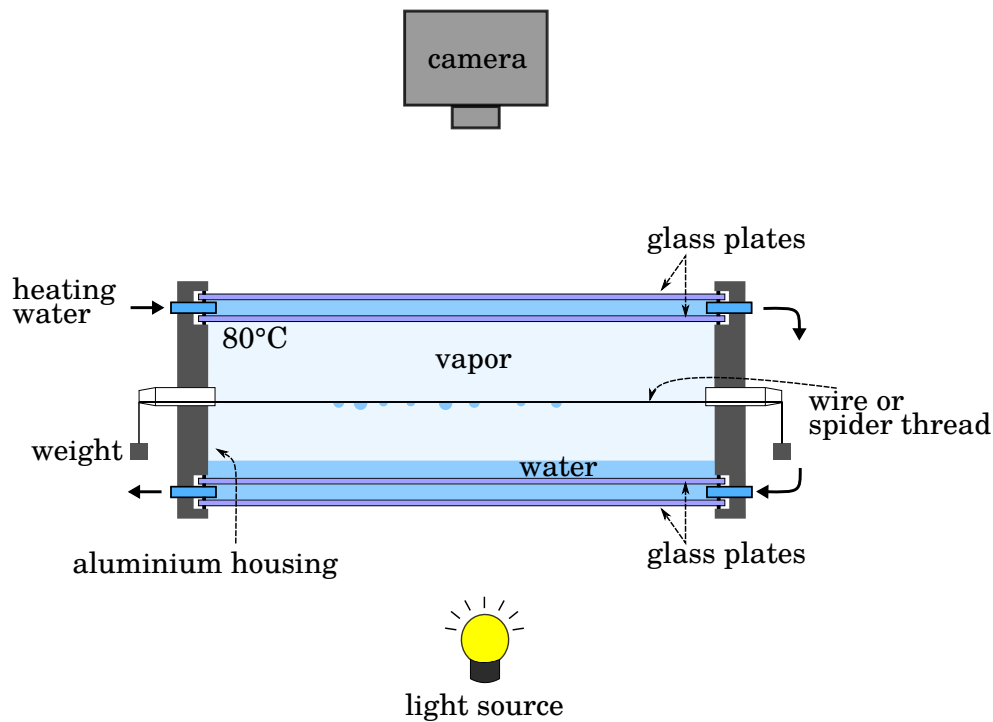
Figure 1.4.: Sketch of the setup developed for an experimental analysis of droplets on a line.

The basic concept of the experiment is sketched in figure 1.4. A string is stretched through a chamber filled with enough water to establish an supersaturated environment when heated. The temperature of the system is controlled via an external thermostat which pumps water of some constant temperature in a loop around the chamber. At first the water goes along the top of the chamber, then along its bottom and in the end back to the thermostat. This way the top of the chamber is slightly warmer than its bottom which prevents condensation on any other surface than the string. Still, if the system is analyzed for continuously changing saturation levels and therefore continuously changing temperatures, lowering the temperature should happen carefully. Otherwise condensation on the top of the chamber could occur. That could corrupt the measurements by droplets dripping onto the string, or by blurring the vision onto the string, lowering the precision of the image detection. Besides controlling the temperature of the system it is also possible to vary the physical and chemical properties of the string.

1.3. Phenomenology

This section introduces the basic physics used for the modeling of breath figures and it introduces the main regimes of droplet growth, as observed in experiments [8, 12].

1.3.1. Wetting of the substrate

Besides the droplet distribution on a surface another quantity which controls the surface coverage is the contact angle formed between a droplet and the surface. It reflects the different surface tensions γ between the liquid, the medium that contains the vapor (which is air in most cases) and the surface. The contact angle θ_C, which minimizes the free energy of the system, can be calculated via YOUNG's equation [13]:

Figure 1.5.: Sketch of a liquid drop (spherical cap, radius of curvature r) showing surface tensions between the three involved phases solid, S, liquid, L, and gas, G respectively.

$$\gamma_{\text{LG}} \cdot \cos(\theta_{\text{C}}) = \gamma_{\text{GS}} - \gamma_{\text{LS}} \qquad (1.1)$$

For droplets on a string one can derive a dimensionless equation for the shape $f(x)$ of the droplet [14] (see sec. A.2):

$$\sqrt{1 + f'^2} + M \cdot f = \frac{d}{dx}\left[\frac{f \cdot f'}{\sqrt{1 + f''^2}}\right].$$

This equation only depends on the dimensionless variable $M = \frac{\varsigma \cdot E}{\gamma_{LG}}$, which is the product of the elongation E of the droplet and the chemical potential ς divided by the surface tension γ_{LG} between the liquid phase and the gas phase. Due to the surface tension the droplet will form a rotational ellipsoid, so $f = \alpha \cdot \sqrt{1 - x^2}$. The variable α determines the vertical extension of the droplet and therefore influences M:

$$M = -\frac{1}{\alpha} - 1.$$

For a realistic string we also need to consider its thickness ρ. Using eq. 1.1 in the limit of $\rho \to 0$ and $\alpha \simeq 2$ leads to an explicit equation for the contact angle θ_C:

$$\theta_C = \frac{\pi}{2} - \frac{\rho}{2 \cdot E}. \qquad (1.2)$$

So large droplets form a contact angle $\frac{\pi}{2}$ whereas small droplet form a flatter one making them grow relatively faster.
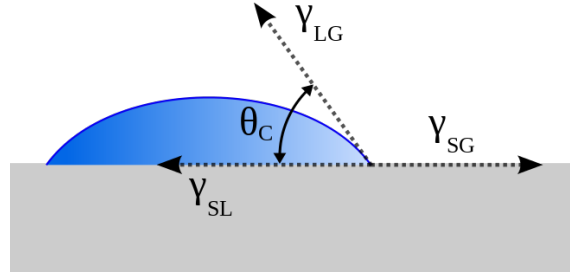
1.3.2. Growth regimes

For the growth of droplets on an initially free surface there are four characteristic stages for which the main growth processes follow different laws [12]:

1. **Nucleation** and growth **of new droplets on the free surface**. These droplets are so small and are separated so far away from each other, that they do not influence their neighbours. Consequently, the growth rate depends only on the flux of vapor. If that flux is constant over time we get a direct time dependence of the droplet size which can be written as

$$r \sim t^{\nu}.$$

   The constant ν depends on the microphysics of droplet growth in our system. If the growth rate is limited by diffusion then $\nu = 1/4$ and if it is limited by the flux then $\nu = 1/3$ [15].

2. As the droplets grow they eventually come into contact and merge. This is the **coalescence regime** where the mono-disperse distribution starts to change but still is mostly uniform. The reason is the small amount of space on the substrate released when two neighbouring droplets merge. It is too small for new droplets to nucleate. So there is no nucleation of new droplets [8, 10]. This leads to a roughly mono-disperse size distribution:

$$n(s,t) \sim s^{-\theta} f^{*}\left(\frac{s}{S(t)}\right)$$

   where f^{*} denotes a characteristic asymptotic shape of the distribution and $S(t)$ is the typical droplet size.

3. With the size of the droplets also the area that is released when two droplets merge grows bigger. If this area is big enough new droplets start to nucleate there as seen in fig. 1.3(b). A **self-similar pattern of droplet** emerges. This leads to a new characteristic shape of the distribution $n(s,t)$ with a power-law tail of $f(x)$ towards small droplet sizes [8, 9, 11]:

$$n(s,t) \sim s^{-\theta} f\left(\frac{s}{S(t)}\right) \quad \text{with} \quad S(t) \sim t^{z}.$$

4. The last regime is reached when the first **droplets start to feel gravity**. Then they drip off, when suspended from a horizontal substrate. Otherwise they either flow down and take smaller droplets with them or just deform so that they no longer have the same shape as the smaller droplets (see fig. 1.3(a)). This rather complicated case has

also been observed [16, 17] but is of minor interest for the present work, where no droplet dripping will be considered.

The present work will mainly analyze the self-similar droplet distribution and related observables like the covered area or the droplet density.

1.4. Outline

The present work will analyze the size distribution of three dimensional droplets on a one dimensional substrate using data obtained by a numerical modeled system. Therefore we will discuss the theoretical background in chapter 2. This includes mainly an approach using scaling theory with an additional fractal packings ansatz. These are used to derive theoretical expectations for the main observables of the system, including the porosity, the number of droplets and the droplet size distribution. Here we especially focus on the distribution of small sized droplets and the influence of different interaction mechanisms and volume fluxes. Chapter 3 then will lay down the basic concepts of the simulations algorithms. Furthermore the changes to achieve different dynamics are explicitly discussed. A main part is the introduction of the droplet interaction range I.

In the last part we then analyze the data obtained from the simulations. In chapter 4 the time evolutions of the porosity and the number of droplets are compared for different microdynamics. Using results for the scaling exponents obtained by the theoretical treatment and the data for the porosity we rescale the droplet size distribution in chapter 5 to present a uniform description for all data.

2. Revisiting the scaling theory

In the following the theoretical basis for this work will be laid. The whole section is based upon work from and discussions with my supervisor Prof. Dr. Jürgen Vollmer [14].
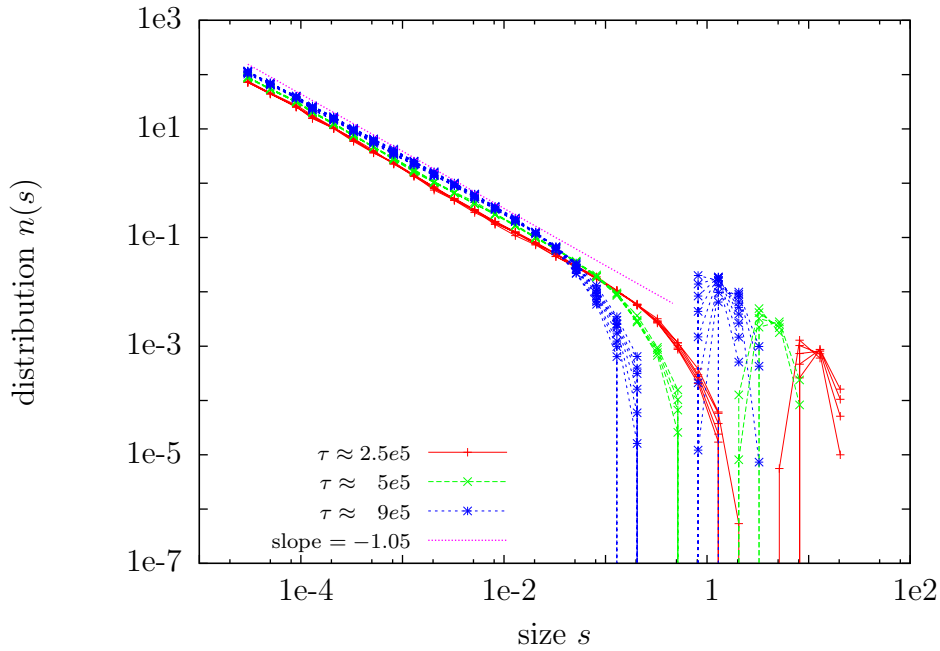
2.1. Dimensionless units

Figure 2.1.: Droplet size distribution at different times τ in regime 3.

From the power-law distribution of small sized droplets we observe in fig. 2.1 we deduce a self-similar droplet distribution in regime three. To analyze this distribution we use dimensionless quantities. The quantities of interest are the time t, the total volume V deposited on the surface, the number of droplets occurring N, which already is dimensionless, and the total covered length L. To measure the quantities we use the fact that there is a smallest droplet size s_0 of droplet sizes appearing in the system. The length is measured by the diameter d_0 of those smallest droplets, so that $L' = L/d_0$ is the dimensionless length scale. The volume is measured in units of the smallest droplets, so that $V' = V/s_0$. Our model describes the volume flux Φ onto the surface as independent of the surface state (more precisely: on

the number of droplets and their size), and that it is constant over time. Let t_0 be the time needed to deposit a droplet of size s_0 on an area of size $c \cdot d_0 = c \cdot 2 \cdot r_0$. Then $s_0 = c\,r_0^3$ and

$$\Phi \cdot t_0 \;=\; \frac{s_0}{c \cdot 2 \cdot r_0} = \frac{r_0^2}{2}.$$

Adopting t_0 as our time unit we arrive at the dimensionless time scale

$$\tau = \frac{t}{t_0}.$$

2.2. Scaling ansatz

Now, we observe that the evolution of the self-similar distribution is completely characterized by the characteristic size $S(\tau)$ of the biggest droplets in the system. This should be growing in time, so we assume:

$$S(t) \sim \tau^z \quad \Leftrightarrow \quad r(\tau) \sim \tau^{z/D}, \tag{2.1}$$

where D is the dimension of the drop, $D = 3$. Analogously d is the dimension of the substrate, $d = 1$. Moreover, when the droplets grow larger the number $n(\tau)$ per unit substrate area decreases in time:

$$N(\tau) = \int ds\, n(s,\tau) \sim \tau^{-z'}. \tag{2.2}$$

To get an expression for $n(s,\tau)$ we use the scaling ansatz from FAMILY and MEAKIN [10, 18] which is a consequence of the *Buckingham-π-theorem*:

$$n(s,\tau) = s^{-\theta} \cdot f\left(\frac{s}{S(\tau)}\right) \tag{2.3}$$

In fig. 2.1 we see, that the only time dependent part is the distribution of the largest droplets. All other aspects of the distribution can be described by a power law and cut-offs for small and big droplet sizes.

2.3. Volume

The total volume $V(\tau)$ is obtained by a summation of all droplets multiplied with their size. Since we sum over a large system it can be approximated by an integral, starting from the size of the smallest drops:

$$V'(\tau) \;=\; \int_{s_0}^{\infty} ds \cdot s \cdot n(s,\tau). \tag{2.4}$$

Using eq. 2.1 and 2.3 the integral transforms to

$$V'(\tau) \approx \tau^{(2-\theta)z} \cdot \int_{\frac{s_0}{S(\tau)}}^{\infty} dx \cdot x^{1-\theta} \cdot f(x).$$

Where $x = \frac{s}{\tau^z}$. With the assumption, that for $\lim_{x \to 0} \frac{f(x)}{x^{\theta-1}} = 0$ the integral becomes a time independent constant. Since we have a constant volume flux, V' is proportional to τ. Hence, eq. 2.4 provides the condition:

$$1 = (2 - \theta)z. \tag{2.5}$$

2.4. Covered length

Another relation between the exponents is obtained by observing the over-all covered length L', which should approach a constant in time for the asymptotic regime. It is given by the integral over the surface space a_s covered by each droplet. Using $a_s = c \cdot s^{\frac{d}{D}}$: we can write down an expression for L':

$$
\begin{aligned}
L'(\tau) &= c \cdot \int_{s_0}^{\infty} ds \cdot s^{d/D} \cdot n(s, \tau) \\
&= c \cdot \tau^{(\frac{D+d}{D} - \theta)z} \cdot \int_{\frac{s_0}{S}}^{1} dx \; x^{\frac{d}{D} - \theta} \cdot f(x).
\end{aligned}
\tag{2.6}
$$

Where again $x = \frac{s}{t^z}$. Assuming now, that for $\lim_{x \to 0} f(x) \cdot x^{\frac{d}{D} - \theta} = 0$ the integral becomes a time independent constant, the requirement leads to another equation for z and θ:

$$0 = (\frac{D+d}{D} - \theta)z,$$

Using eq. 2.5 and $d = 1$, $D = 3$ we find

$$\theta = \frac{4}{3} \text{ and } z = \frac{3}{2}. \tag{2.7}$$

2.5. Number density

Fig. 2.2 shows, how the droplet size distribution looks like if it is rescaled with the ansatz of eq. 2.3, using the derived values for θ and z. We observe a data collapse for all but the smallest droplets. The resulting characteristic shape can be approximated by some new power law plus a lower and an upper cut-off, depending only on the size of the smallest droplets and of the biggest ones. By that means, we have to drop the function $f(\frac{s}{S(\tau)})$ from
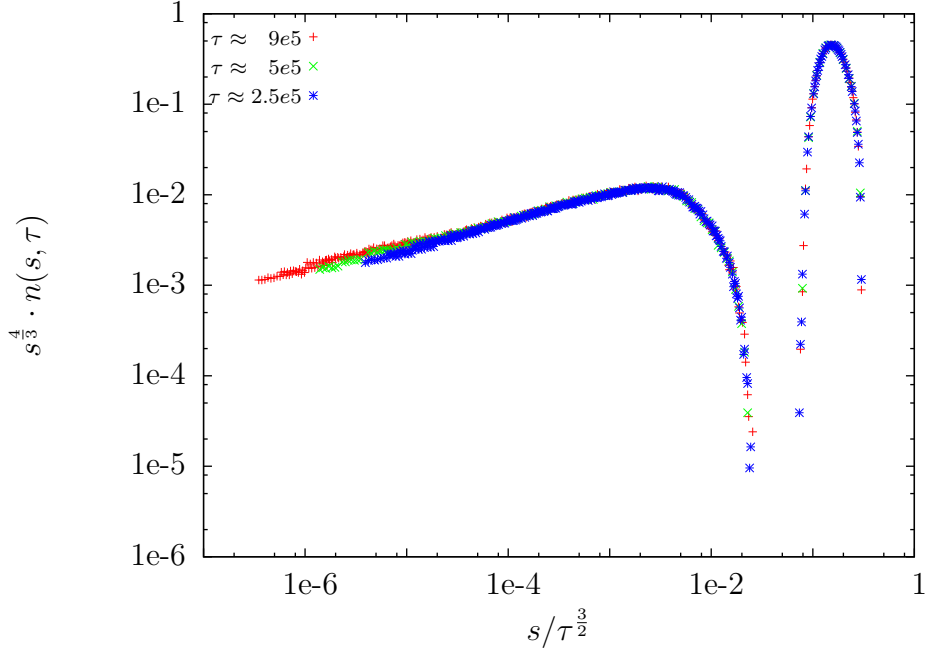
2. Revisiting the scaling theory

Figure 2.2.: Rescaled droplet size distribution at different times τ in regime 3. Here $\theta = \frac{4}{3}$ and $z = \frac{3}{2}$ were used to plot $s^\theta n(s,\tau)$ over $s/S(\tau)$, with $S(\tau) \sim \tau^z$.

eq. 2.3 and redefine it by considering distribution of droplets on the substrate as a fractal packing of discs [9]:

$$f(s, S(\tau), s_0) = \left(\frac{s}{S(\tau)}\right)^\epsilon \hat{f}\left(\frac{s}{S(\tau)}\right) \hat{g}\left(\frac{s}{s_0}\right), \tag{2.8}$$

whereby ϵ is the new power-law exponent describing the systems fractal dimension. The function $\hat{f}(x) \sim 1$ for $x < 1$ and is zero for $x \gtrsim 1$. Hence it provides a cut-off for the large droplets. In a similar way $\hat{g}(x)$ provides a cut-off for the small droplets. It is one for $x > 1$ and it is zero for $x < 1$ after s_0 is the size of the smallest existing droplets in the system.

To determine the new exponent ϵ we consider the time evolution of the total number of droplets. In the self-similar regime, this should decrease according to $N(\tau) \sim \tau^{-z'}$, with a positive contact z'. Using eq. 2.8 leads to:

$$
\begin{aligned}
\tau^{-z'} \sim N(\tau) &= \int_0^\infty ds \ s^{-\theta} \cdot \left(\frac{s}{\tau^\alpha}\right)^\epsilon \hat{f}\left(\frac{s}{\tau^\alpha}\right) \hat{g}\left(\frac{s}{s_0}\right) \\
&= \tau^{z(1-\theta)} \cdot \int_{s_N/\tau^z}^1 dx \ x^{\epsilon-\theta} \ \hat{f}_0 \\
&= \frac{\tau^{z(1-\theta)} \hat{f}_0}{\theta - 1 - \epsilon} \cdot \left[\left(\frac{N_0}{\tau^z}\right)^{\epsilon-\theta+1} - 1\right] \\
&= \frac{s_N^{\epsilon-\theta+1} \hat{f}_0}{\theta - 1 - \epsilon} \cdot \tau^{-z\epsilon} \quad \text{for} \quad \epsilon > d/D \quad \text{and} \quad \tau \gg 1.
\end{aligned} \tag{2.9}
$$

Here s_N characterizes the upper boundary for the influence of $\hat{g}(s/s_0)$. So we get a connection

between z' and the scaling exponent ϵ:

$$z' \;=\; z\epsilon \;=\; \frac{3}{2}\epsilon. \tag{2.10}$$

2.6. Porosity

Another observable that will be used to analyze the system is the fraction of non-wetted area, the porosity $p(\tau)$. It can be determined via the number of droplets per unit area $n(\tau)$. Introducing the *mean gap size* β per droplet, which is considered to be constant in time at least in the asymptotic regime, and the interaction range I, determining the minimal distance between two droplets; we find

$$
\begin{aligned}
P(\tau) \;&=\; 1 - A(\tau) \\
&=\; 1 - \int_0^\infty ds\,(I + 2s^{d/D})s^{-\theta}\,f\!\left(\frac{s}{S}\right) \\
&\simeq\; 1 - I\,N - \left[1 - I\,N - \int_0^{\frac{s_N}{S}} dx\,x^{-1}\hat{f}_0\,x^\epsilon\right]) \quad \text{for} \quad \tau \gg 1 \\
&=\; \frac{\hat{f}_0}{\epsilon}\left(\frac{s_N}{S}\right)^\epsilon \;\sim\; \tau^{-z'} \\
&=\; \beta \cdot n(\tau)
\end{aligned}
\tag{2.11}
$$

2.7. Lower cut-off function

To determine the lower cut-off $\hat{g}$ of the scaling function we have to focus on the distribution of the small sized droplets. The following derivation stays closely to the derivation of Vollmer et al. [9] for a system of three dimensional droplets on a two dimensional substrate.

The total volume V of all droplets is the most stable observable. By construction of our algorithm it grows linear in time. Consequently, we rewrite eq. 2.3 and 2.8 in form of a volume:

$$s\,n(s,\tau) = S^{-\frac{1}{3}}\left(\frac{s}{S}\right)^{\epsilon-\frac{1}{3}}\hat{f}(s/S)\,\hat{g}(s/s_0)$$

Based on the work on two dimensional breath figures [9] we expect that the scaling exponent ϵ and the cut-off function $\hat{g}$ are not universal. Rather $\hat{g}$ depends on the rules of local droplet growth. To establish that relation we follow the evolution of droplets smaller than s_* over a time interval $[t : t + dt]$ whereby the infinitesimal element dt and the considered section are chosen such that no merging of drops larger than s_* will occur. Choosing $s_* \ll S$ we may assume that $\hat{f}(s_*/S) \to \hat{f}_0$ = constant. The volume for this part of the distribution then

amounts to:

$$V(s_*) = \int_{s_0}^{s_*} s \, n(s,\tau) \, ds = \frac{\hat{f}_0}{S^{\frac{1}{3}}} \int_{s_0}^{s_*} \left(\frac{s}{S}\right)^{\epsilon - \frac{1}{3}} \hat{g}(s/s_0) \, ds.$$

An infinitesimal increase of s_* simply means increasing the upper limit of the integral to $s_* + (\dot{s} \, dt)$:

$$\frac{dV}{dt} = \frac{V(s_* + \dot{s} \, dt) - V(s_*)}{dt} = \frac{\hat{f}_0}{S^{\frac{1}{3}}} \left(\frac{s_*}{S}\right)^{\epsilon - \frac{1}{3}} \hat{g}(s/s_0) \, \dot{s}$$

We also know that the volume can only change due to the flux onto the considered section of size Σ which solely depends on s_* and S. We approximated Σ using the fractal packings approach from eq. 2.8:

$$\frac{dV}{dt} = \Sigma(s_*, S) \, \Phi \; \sim \; \left(\frac{s_*}{S}\right)^{\epsilon} \Phi.$$

Dropping for convenience the $*$ in s_* we hence find

$$\hat{g}(s/s_0) \sim \frac{\Phi}{\hat{f}_0} \frac{s^{1/3}}{\dot{s}}. \tag{2.12}$$

As mentioned in sec. 1.3.2 the growth of large droplets follows the equation $\dot{s} \sim \Phi \, s^{1/3}$. For smaller droplets a sub-dominant contribution involving the size of the smallest occurring droplets, $s_0^{1/3}$ becomes noticeable,

$$\dot{s} \simeq \Phi \left[s^{1/3} + s_0^{1/3} \right] = \Phi \, s^{1/3} \left[1 + \left(\frac{s_0}{s}\right)^{1/3} \right]. \tag{2.13}$$

Here also those newly added droplets are included in the growth of another droplet that are placed close enough to this droplet to get directly absorbed. So we find an explicit expression for the function $\hat{g}$:

$$\hat{g}\left(\frac{s}{s_0}\right) = \frac{\hat{f}_0^{-1}}{1 + a(\frac{s}{s_0})^{-b}}. \tag{2.14}$$

where $\alpha = 1$ and $b \simeq \frac{1}{3}$ according to eq. 2.13, and deviations from these values can account for non-trivial correlations arising from the influence of neighbouring droplets.

2.8. Varying droplet growth laws

Up to this point the theory was tailored to reflect a specific scheme to grow the droplet volume. The dynamics of coalescence followed the rule *merge upon impact* or alternatively,

when the distance falls below some constant value called *interaction range I*. Another option is to choose I to be proportional to the radius of a droplet or to choose the volume flux to be homogeneously distributed over the surface of the substrate. The following section concentrates on the expected changes in the systems behaviour if those changes are adopted.

2.8.1. Radius dependent interaction range

To understand the behaviour of a system with a droplet interaction range proportional to the radius of a droplet, where λ defines the proportionality, we redefine porosity of the system:

$$\begin{aligned} \tilde{p} &= 1 - (1 + \lambda)\, a = 1 - (1 + \lambda) \cdot (1 - p) \\ &= (1 + \lambda)\, p - \lambda \end{aligned} \tag{2.15}$$

Since the porosity is calculated via an integral over the radius distribution the prefactor $(1 + \lambda)$ can be interpreted as a deformation of the droplet in horizontal direction. The constant term $-\lambda$ contributes to a constant minimal distance between two neighbouring droplets. We see that a system with an interaction range depending on the radius of a droplet is the same as a system with a constant interaction range I but with deformed droplets. Meaning that we no longer look at droplets with a spherical shape but rather at droplets in form of rotational ellipsoids. So $\tilde{p}$ should provide the same results as for a system with zero interaction range for arbitrary values of λ.

2.8.2. Surface-dependent flux

To deal with surface depending flux the surface of all droplets has to be considered. To cover different growth scenarios in a unified framework, we consider a situation where sufficiently large droplets grow like

$$3\,R^2\,\dot{R} \simeq \Phi\,R^{\tilde{d}} \quad \Rightarrow \quad 3\,R^{D-1-\tilde{d}}\,\dot{R} = \Phi \quad \Rightarrow \quad R^{D-\tilde{d}} = \tau$$

$$S \simeq R^D \simeq \tau^{\frac{D}{D-\tilde{d}}}$$

$$\Rightarrow \quad R \sim \begin{cases} \tau^1 \Rightarrow S \sim \tau^D & \text{if } \tilde{d} = 2 \quad (\text{flux} \sim \text{surface area}), \\ \tau^{1/2} \Rightarrow S \sim \tau^{D/2} & \text{if } \tilde{d} = 1 \quad (\text{flux} \sim \text{substrate length}). \end{cases}$$

Then the effective surface area $\sigma = \int ds\, s^{\frac{\tilde{d}}{D}} \cdot n(s, \tau)$ of the droplet follows out of eq. 2.3. Analogously to sec. 2.4 the result is

$$\sigma \sim S^{1 + \frac{\tilde{d}}{D} - (1 + \frac{d}{D})} = S^{\frac{\tilde{d}-d}{D}} = \begin{cases} S^{1/D} & \text{if } \tilde{d} = 2, \\ S^0 & \text{if } \tilde{d} = 1. \end{cases}$$

2. Revisiting the scaling theory

Again we use, that the change of volume is equal to the flux onto the droplets effective size as long as we do not consider any merging events:

$$\dot{V} \;=\; \Phi\,\sigma \;=\; \Phi\,S^{\frac{\tilde{d}-d}{D}} \;=\; \Phi\,\tau^{\frac{D-d}{D-\tilde{d}}-1} \;\Rightarrow\; V \;\sim\; \tau^{\frac{D-d}{D-\tilde{d}}} \begin{cases} \Rightarrow & V \;\sim\; \tau^2 \text{ if } \tilde{d}=2, \\[2mm] \Rightarrow & V \;\sim\; \tau \;\; \text{ if } \tilde{d}=1. \end{cases}$$

We see that as long as we treat the system in terms of V or S we expect no differences (except for ϵ and $\hat{g}$). As far as the scaling relations are concerned the only apparent difference lies in the time dependence of the droplet growth — it scales linear and quadratic respectively. To give a specific example we reconsider the systems porosity:

$$\begin{aligned} \textbf{Porosity} \qquad p \;&=\; 1 - a \;=\; 1 - \int ds\, s^{-\theta}\, s^{d/D}\, f\!\left(\frac{s}{S}\right) \\[2mm] &=\; 1 - \left[1 - \int_0^{\frac{s_0}{S}} dx\, x^{\epsilon + \frac{d}{D} - \theta} \right] \\[2mm] &\sim\; \left(\frac{s_0}{S}\right)^{\epsilon} \;\sim\; S^{-\epsilon} \;\sim\; V^{-\epsilon\frac{D}{D-d}}. \end{aligned}$$
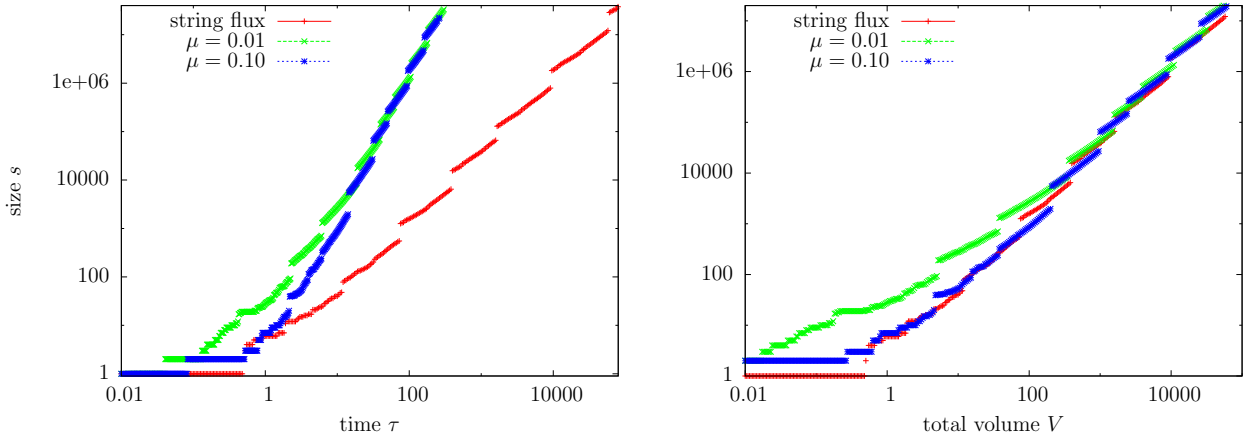

Figure 2.3.: Comparing the asymptotic growth laws for the two different flux types. If plotted against time the surface dependent flux provides an exponent twice as big but plotted against the systems total volume both growth laws are asymptotically the same. μ defines the ratio between the surface of a droplet with unit diameter and a thread of string of unit length and therefore defines the thickness of the string.

3. Simulations

We showed that all quantities are fully described by a set of three exponents θ, z and ϵ or z' and two cut-off functions $\hat{f}(x)$ and $\hat{g}(x)$. Hence it does not matter whether we observe $p(\tau)$, $n(\tau)$ or $n(s, \tau)\ s^\theta$ in the asymptotic regime. The quest now is to find ϵ using data attained by a numerical model of three dimensional droplets on a one dimensional surface. The next section 3.1 describes a program provided by J. Vollmer. The following parts specify the modifications added to it.

3.1. Basic concept

The substantial assumption for the numerics is that there is no difference between the processes of new droplets nucleating on the substrate and the growth of already existing droplets. This simplification allows us to use a volume flux which is constant over the whole system and does not differ for wetted and free areas. Together with the already mentioned dimensionless units this enables a relatively simple, event driven algorithm.

The basic process of the algorithm is to idealize the flux by adding a new droplet to the system in every time step (see fig. 3.1). The volume s_0 of those droplets is defined as 1. It is the smallest possible volume of droplets in the system. This implies, that the total volume V' is equal to the dimensionless time τ which counts the number of droplets added to the system. The radius r_0 of the smallest droplets is defined as 0.5, according to 1.2, so that the length of the system can simply be measured in diameters d_0 of the smallest droplets.
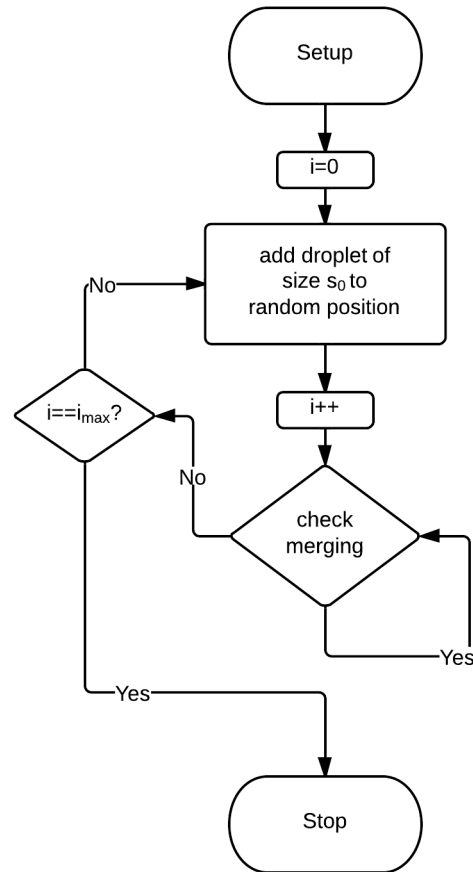

Figure 3.1.: Flow chart for the basic concept of the algorithm.

3. Simulations

To add a new droplet to the system a random point on the surface is chosen as the position of its center and the creation time of the drop is saved. Now it has to be checked if this new drop overlaps with already existing droplets. Since the system is one-dimensional each droplet has exactly two neighbours (because of periodic boundaries) and could only overlap with these two. To keep track of which droplets are adjacent, each droplet contains the information about its neighbours. To achieve these informations for a newly added droplet faster than by going through the system from one side to the other, each one is assigned a node in a binary tree when added. So every time this happens, it is placed in the tree according to its center. To check whether these drops merge the distance of their centers is calculated and their radii and the interaction range are subtracted. If there is merging the procedure is as follows: The older one of the merging droplets is assigned to be kept, since statistically it is the bigger one and its volume is set to the sum of the two old volumes. Its new center is set to the former center of mass and its radius is calculated via $r_{\mathrm{new}} = (r_{\mathrm{old},1}^3 + r_{\mathrm{old},2}^3)^{\frac{1}{3}}$. The node for the other drop is removed from the binary tree and the memory is released. Since time is measured by the total volume of the system, such a merging event is instantaneous. This is a reasonable approximation, considering previous experiments [8].

The program divides its output into four streams. The units for all outputs are the same: Volume is measured via s_0, length via d_0 and time via τ.

1. The first stream provides status informations while the program is running and sends them to the standard output. At the beginning it displays the set of given parameters like the system size and how long it shall run and also the seed for the random number generator. After that, it provides progress informations for logarithmically growing time steps. Since the program also performs a self-consistency check on that time scale there will also be output of these informations if the deviations are bigger than specified threshold values.

2. The second stream saves informations for each droplet in the system on the same logarithmic time scale. These informations are, besides a sequential number and the current time, the time of creation of the given droplet, its volume and the position of its center. This is one of the two most important files the program produces.

3. The third stream records data about the moments of the droplet size distribution: The current time, the total number of droplets, the over all droplet volume (which should be and always is equal to the time) and the total length of wetted area.

4. The fourth channel saves the creation time and center position for each added droplet. For each coalescence the age, position and size of the two contributors and of the merged droplet is recorded. Since this information is not always of interest and since they need a lot of disc space the program provides the possibility to turn off the log-file.
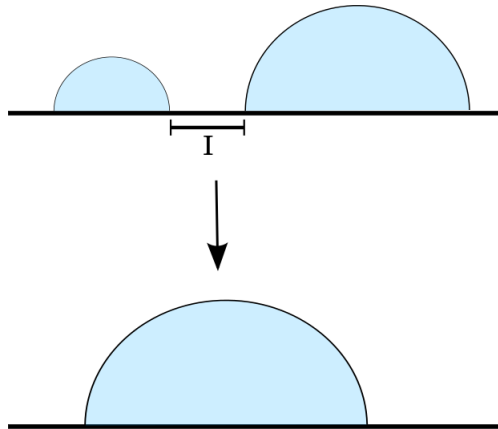
Figure 3.2.: Sketch of the principle for the interaction range.

3.2. Introducing the interaction range

The first change to the algorithm is to introduce an interaction range I for the droplets. It is defined in the way, that as soon as the distance between two adjacent droplets becomes smaller than the interaction range these droplets will merge as shown in 3.2.

Implementation in the code is simply accomplished by subtracting the interaction range from the value used to determine the distance of two droplets.

Another interaction mechanism is already presented in sec. 2.8.1. Instead of a constant interaction range that is the same for all droplets, we introduce an interaction range that is proportional to the radius of a droplet. So it is neither the same for all droplets nor constant in time. Instead it allows larger droplets to grow even faster than smaller droplets compared to the former mechanism since they have a higher merging rate.

The implementation is analogous to the case with constant I. A constant factor λ is introduced that defines the ratio between the radius and the interaction range. As the distance between two adjacent droplets is calculated not the radii of both are taken into account but each radius times $1 + \lambda$.

3.3. Changing the collision rules

The next change of the droplets dynamics does not vary their range but the amount of merging events that can happen in one time step. The original algorithm only allowed for binary events. The first occurs always when a newly added droplet is set inside the range of an older one. If this older droplet thereby becomes large enough to get in contact with a neighbour the second event occurs. However, there are cases where the growing droplet overlaps with both its neighbours. The previous algorithm was designed in the way, that the larger overlap determines the merging partner, since for a non-instantaneous growing of the droplets this one would have been reached first. But then it is also reasonable to assume

that it takes some time after one side of the droplet makes contact until the expansion of the other side is stopped. Therefore a threshold value δ is introduced which allows coalescence with both neighbours as long as the difference in overlap is smaller than δ.

Similarly to the interaction mechanism the model for the flux is varied in two different ways. The first modification keeps the implementation of a homogeneous flux onto the string and just applies when a newly added droplet directly merges. It is now assumed that this is not an event where some small droplet is added to the surface, but where a mass flux onto the surface of the droplet makes it grow. The difference being that for the first case the grown droplet is located in the center of mass of the merging partners. But for the second case the location of the old droplet stays unchanged.

To achieve this change a small section is added to the merging algorithm. It checks whether one of the merging partners was just added. In that case the center of the merged droplet is set equal to the center of the older merging parter (which will be the kept droplet). In every other case the center of mass of the two droplets is calculated and set as the center of the grown droplet.

3.4. Changing the flux

The second modification changes the entire type of the flux. As discussed in sec. 2.8.2 it is made homogeneously distributed over the whole surface of the system, consisting of the surface of all droplets and the surface of the free sections of the substrate. Therefore this surface is mapped onto a line so that the basic concept for adding new droplets remains unchanged: A random point in some given interval is chosen as the center of the new droplet. Hence each droplet needs a new attribute stating the cumulative value of surface area up to its position (measured from the left side of the system). At least if the new droplet should still get added by using the binary tree. This is highly recommended for systems with a huge amount of droplets. The challenge then is to keep the event driven algorithm and also to keep the attribute for the cumulative surface area correct for all droplets since a local change of a droplets' surface effects more droplets than just its neighbours. Therefore not the absolute cumulative surface up to a droplet is stored but the difference to its father in the tree. Hence a local change of surface area only affects the path in the binary tree leading to this point on the surface rather than all droplets to the right of this position.

This is an easy task when adding a droplet since in that case the droplets path in the binary tree is followed anyway. Thus, every time the path changes its direction (left or right child node) the cumulative value of the current drop has to be updated. It becomes more complicated when two droplets are merging: Now two different paths have to be updated. Since both paths can contain an intersecting set of droplets we have to distinguish between the path of the droplet which is kept and growing and the path of the droplet to be removed.

For the first one we just calculate the difference in surface area and then follow the tree up to its top, updating every time the path changes its direction. The second case is the troubling one: When a droplet is removed its node has to be taken out of the tree to keep it effective. If the tree already contains a lot of nodes this procedure often involves the restructuring of a subsection of the tree. Then the cumulative value for all involved nodes has to be updated correctly.

Additionally, every time a droplet is added or a merging event takes place the surface area of the whole system is updated too. This provides a straightforward control mechanism to check whether the corrections were calculated properly: Each time the systems moments are calculated also the overall surface area is determined via each droplets surface and the distance between all droplets. Both results are then compared.

Since the thickness of the substrate is important for the total surface of the system we introduce the variable μ. It defines the relation between the surface area for a section of substrate with unit length to the surface of droplet with unit diameter d_0.

4. Porosity and the number of droplets

4.1. Zero interaction range

We first set the value for the interaction range to zero, and see how the system size and the simulation time influence the droplet size distribution. To that end the first simulations were done for different system sizes, in the range of 10^3 to $5 \cdot 10^4$, and different maximal running times, in the range of 10^2 to 10^4.

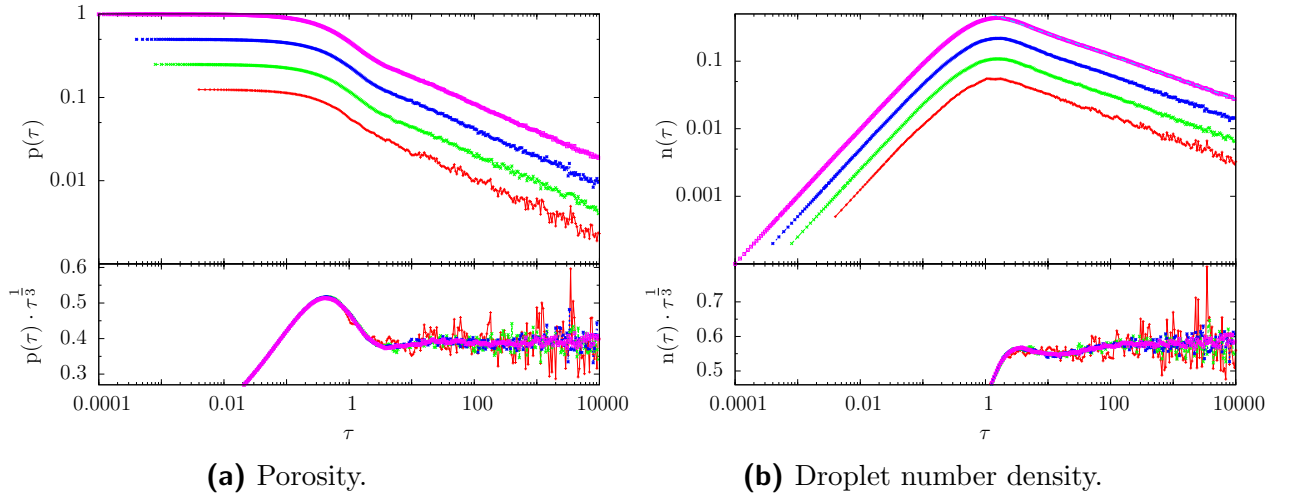

(a) Porosity.

(b) Droplet number density.

Figure 4.1.: Influence of the systems length onto the porosity and the number of droplets. The lengths of the shown systems are from bottom to top: $1e3, 5e3, 1e4, 5e4$. The upper curves are plotted equidistant on a logarithmic scale, in fact the data collapses. The curves below show the data rescaled with an estimated exponent $z' \approx \frac{1}{3}$.

Fig. 4.1 shows the time evolution of the total number of droplets and the porosity. Since time is normalized by the unit surface an increase of the system length corresponds to a reduction of the initial value of τ. The noise of the data becomes bigger the longer the program runs and the smaller the system is. Knowing that, the noise in the reduced plots can be explained by the higher accuracies of the bigger systems.

Furthermore, we can well observe the previously introduced growth regimes:

1. **regime** — At first the number increases linearly with a slope of 1, which corresponds to the regime where the droplets not yet interact.

2. **regime** — As τ goes to one, the growth decreases and passes over into a maximum
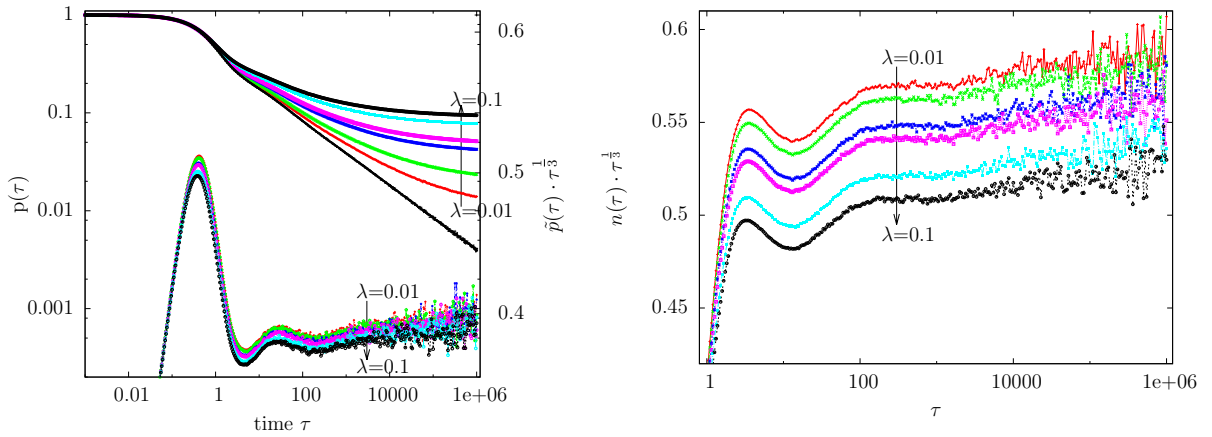
4. Porosity and the number of droplets

after which the droplet number starts to decrease. The droplet collisions become noticeable but no new nucleation is observed. Analogously the porosity starts decreasing rapidly until it changes to some flatter decrease.

3. regime — Finally an asymptotic behaviour with a different power law evolves. This transition happens due to the fact, that nucleation is again possible.

As a final result of these first series of measurement we find a mean slope of $z' = \epsilon z = 0.33$:

$$\epsilon = \frac{2}{3} \cdot 0.33 = 0.22.$$

4.2. Different interaction mechanisms

(a) Porosity. Upper curves belong to left y-axis, curves below to the right y-axis.

(b) Droplet number density.

Figure 4.2.: Influence of a radius dependent interaction range I onto the time evolution of the porosity and the droplet number density. λ is the proportionality factor between the radius and the interaction range: $I = \lambda \cdot R$. Left below: Redefined porosity, rescaled with $z' = \frac{1}{3}$. Right: Droplet number density rescaled with $z' = \frac{1}{3}$.

At first we analyze the radius dependent interaction range. As shown in the upper half of fig. 4.2(a) the porosity p does no longer approach the power-law behaviour for the large τ asymptotics. However, if we use the redefined porosity as suggested in eq. 2.15 we find a perfect collapse of data (black line) for all values of the proportionality factor λ. This curve is identical to the one observed for a system without interaction range. So the exponent for its asymptotics is roughly $\frac{1}{3}$. Therefore the lower half of fig. 4.2(a) shows the porosity rescaled with a factor of $\tau^{1/3}$ and with a non logarithmic y-axis. We observe, that the redefined porosities do not collapse perfectly but that there are some slightly differences in magnitude which follow the variation of λ. The same observation is made for the total number of droplets n (fig. 4.2(b)). It is also rescaled with $\tau^{1/3}$ and plotted on a non-logarithmic y-axis. Yet the effect of λ onto the magnitude of n seem to be slightly stronger than for p.

Both plots also suggest that $\frac{1}{3}$ is no accurate approximation for z' but that it is rather slightly smaller. On a first glance there also seems to be a transition in the power-law exponent between $\tau = 10^3$ and $\tau = 10^4$. However, a closer examination suggest that it is rather due to a damped oscillation around the final asymptotic value.
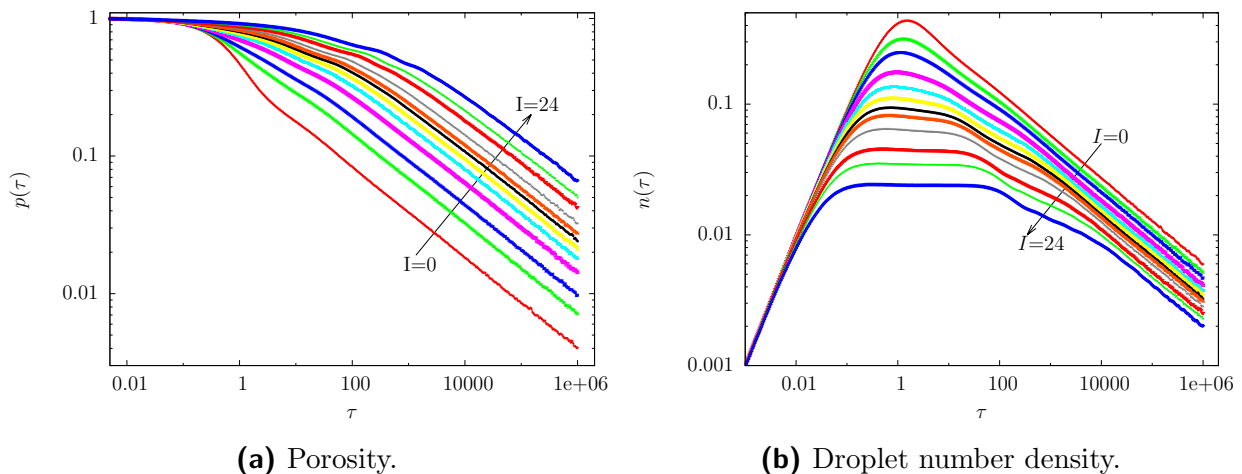

(a) Porosity.   **(b)** Droplet number density.

Figure 4.3.: Influence of a constant interaction range I onto the time evolution of the porosity and the number of droplets.

Even more pronounced shifts for both, the porosity and the droplet number, are presented in fig. 4.3 for a system with constant interaction range I for all droplets. Reconsidering eq. 2.15 explains this connection. Taking into account the interaction range in the porosity there is a constant offset of $-\lambda$, irrespective of the droplets radii. This not only explains the different directions of the shift in the porosity plots when comparing the lower curve of fig. 4.2(a) to fig. 4.3(a), but also the differences in magnitude. The reason is that we only considered $0 < \lambda \leq 0.1$ but $I \in [0, 24]$. More striking is the huge effect onto the intermediate time regime. Especially for n which changes barely for a time interval that is growing with increased I.

This transient region is also the only point indicated by a rough estimation of the differences between the former system, where a droplet was only capable of two merging events per time step, and a system where also merging with both neighbours at the same time is possible.

A more precise comparison reveals a more drastic effect of the modified interaction mechanism. Figures 4.4(b) and 4.5(b) show that a major change occurs in the exponent z'. It is even debatable whether or not the system approaches a power law at all on the considered time scales. Especially for higher values of I the curves are obviously bent.

Another notable observation in fig. 4.4(b) and 4.5(b) is the remarkable similarity of the data for the two different threshold values $\delta = \{0.01, 0.1\}$ that determine the maximal difference in overlap up to which still merging with both neighbours takes place. The reason

4. Porosity and the number of droplets

probably lies in discrete increase of the droplet size[1].
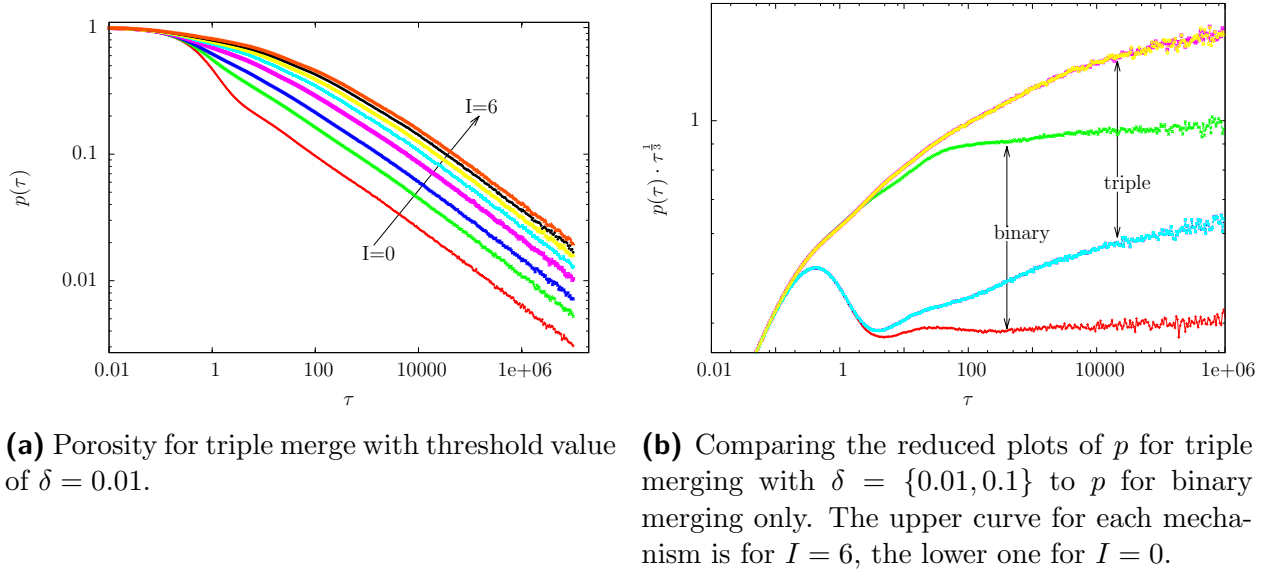
(a) Porosity for triple merge with threshold value of $\delta = 0.01$.

(b) Comparing the reduced plots of p for triple merging with $\delta = \{0.01, 0.1\}$ to p for binary merging only. The upper curve for each mechanism is for $I = 6$, the lower one for $I = 0$.

Figure 4.4.: Influence of a constant interaction range I onto the time evolution of the porosity if a droplet is allowed to merge with both neighbours at the same time.
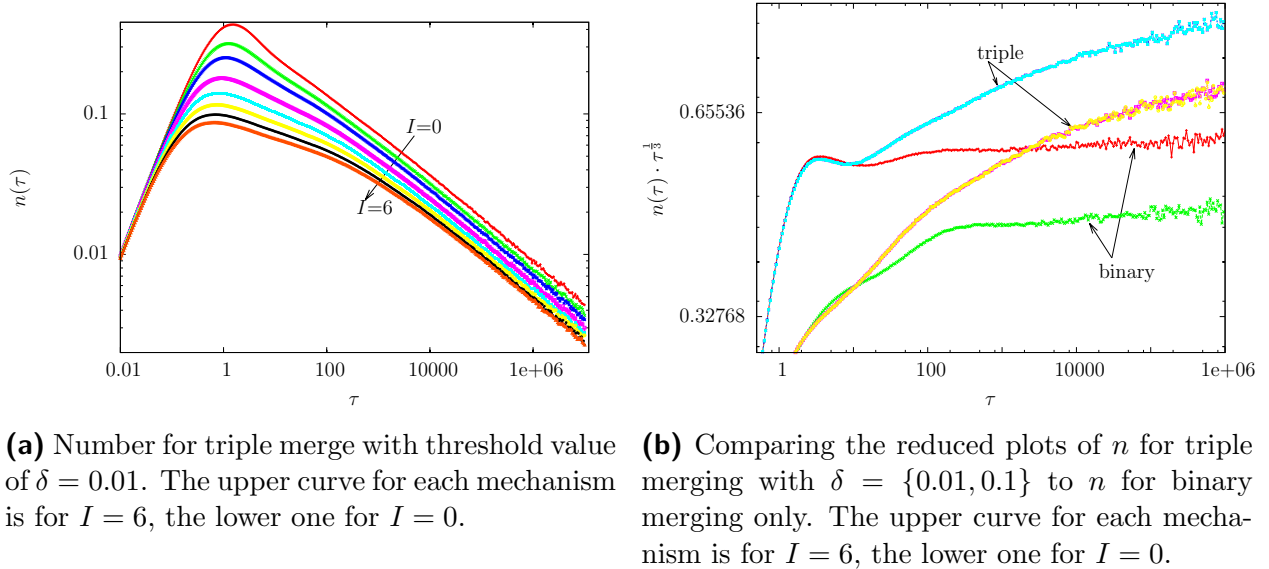
(a) Number for triple merge with threshold value of $\delta = 0.01$. The upper curve for each mechanism is for $I = 6$, the lower one for $I = 0$.

(b) Comparing the reduced plots of n for triple merging with $\delta = \{0.01, 0.1\}$ to n for binary merging only. The upper curve for each mechanism is for $I = 6$, the lower one for $I = 0$.

Figure 4.5.: Influence of a constant interaction range I onto the time evolution of the number of droplets if a droplet is allowed to merge with both neighbours at the same time.

---

[1]In a rough analysis for a series of different δ values we found a series of discrete changes.

4.3. Changing the flux

When newly added droplets do not shift the center of mass when directly added to existing droplets it has no major impact onto the porosity and the droplet number density as we see in fig. 4.6. Both the small and the large time asymptotic behaviour is not influenced. The only deviations are small shifts in magnitude in the second regime of growth.
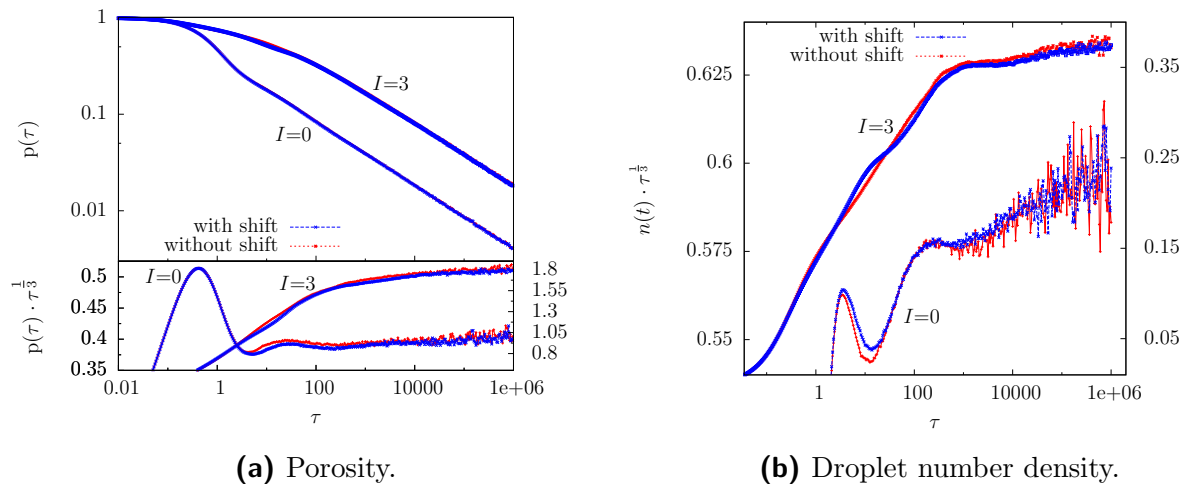

(a) Porosity. **(b)** Droplet number density.

Figure 4.6.: Changes in the porosity and the droplet number density when newly added drops no longer shift existing drops on if they immediately merge. Comparing data for two different constant values of I.

The most drastic differences occur when the flux is changed from substrate length to surface dependency. Although there is no difference in the systems behaviour for early timesteps fig. 4.7 shows that for the large τ asymptotics a completely different scaling exponent z' is observed. Compared to that change and the influences the previously discussed modifications had the differences in the transient region are kind of small.
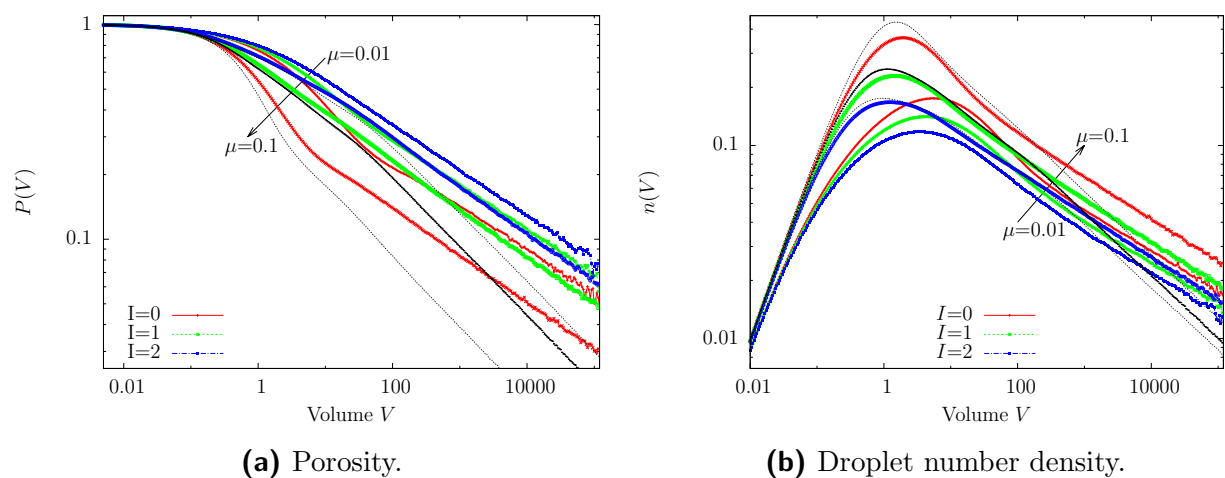

(a) Porosity. **(b)** Droplet number density.

Figure 4.7.: Influence of a constant interaction range onto the porosity and number of droplets for a system with homogeneous flux onto the total surface.

27

4. Porosity and the number of droplets

It is observed, that the shift in the magnitude when varying I seem to depend on the weighting factor μ which determines the surface area of substrate section with unit length compared to the surface of a droplet with unit diameter d_0. The smaller μ the smaller are the shifts. A probable explanation lies in the fact, that with lesser weighting of the substrates' surface also the amount of empty substrate due to the interaction range of the droplets is weighted less and therefore has a reduced influence.

4.4. Influences on the scaling exponents

In sec. 1.2 the theoretical derivations from Blackman and Brochard [11] concerning the scaling exponent $\theta - \epsilon$ were stated, which claimed that it is only depending on the dimensions of the droplets and the substrate but not on any other system properties. However, the results of Blaschke et al. [9] do not fit Blackmans prediction for two dimensional substrates. Therefore we examine the behaviour of $\theta - \epsilon$ in the discussed systems and whether it fits Blackmans results of $\theta - \epsilon = 1.17$.
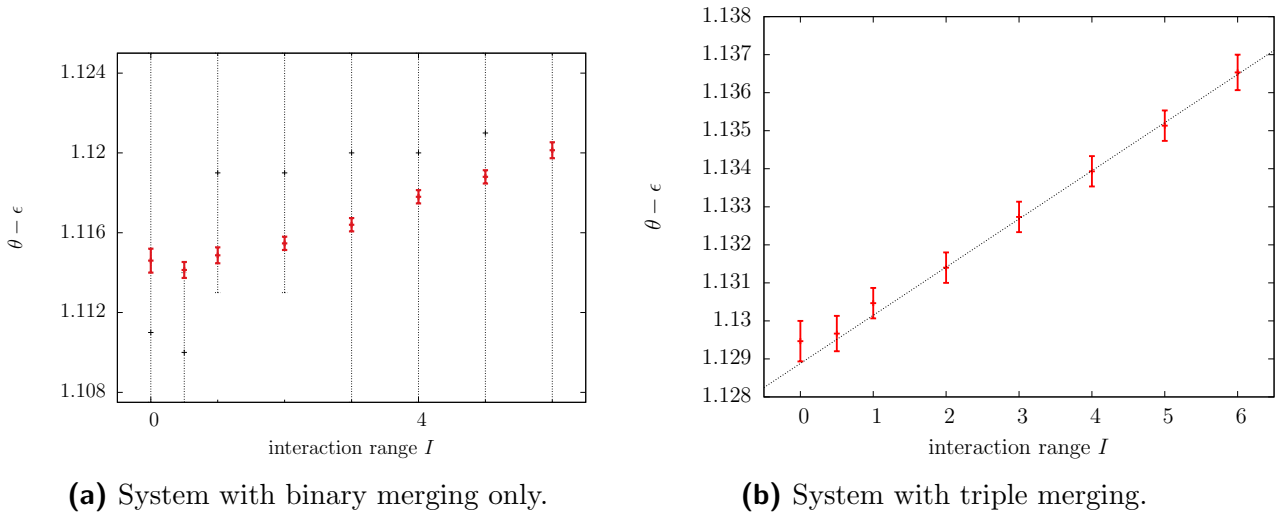

(a) System with binary merging only.   **(b)** System with triple merging.

Figure 4.8.: Scaling exponent $\theta - \epsilon$ obtained for different constant values of I and by fitting the slope to data averaged over 20 simulations. The fitting range for all graphs is $1e4 < \tau < 1e6$.

Analyzing the porosity and the droplet number not only gives more insight into the systems dynamics. Regarding eq. 2.10 it also provides a method to determine the scaling exponent ϵ out of the asymptotically approached power-law exponent z'. Fig. 4.8 shows the results attained by fitting a power law to the last to decades ($\tau = 10^4$ to $\tau = 10^6$) of the porosity data for systems with different, constant interaction ranges. All systems have the same substrate length (10^5) and the data is averaged out of simulations for 20 different seeds for the random number generator. It shows a clear trend that larger values of I give rise to increasing values of $\theta - \epsilon$. In particular for larger values of I the relation is nearly linear

(cf. fig. 4.8)[2]. In contrast, for small I the relation is non-trivial. The black dots in fig. 4.8 represent a finite-size scaling analysis of z' in form of $z'(I, \tau) = z'_\infty(I) - \alpha \cdot \tau^\beta$ which was motivated by fig. 4.4. There a declining curvature is visible for the data of the self-similar region, assuming that it tends towards some limit value τ_∞. Expecting the same behaviour for the system with binary merging but with less magnitude we see that this ansatz does not lead to more precise results but rather enlarges the uncertainties. This may result out of ongoing oscillations of the exponent.

For the triple merging system the I dependence of the exponent is even more pronounced. Although it is not completely certain whether the exponents would converge further for later time steps it strengthens the assumptions of a linear connection to the interaction range. And we also observe that there is no overlap in the range of the exponents covered by the binary and the triple merge system. However, the slopes for the linear approximation are nearly the same ($\approx \frac{1}{75}$) for the triple mering system as well as for the binary merging one.

The results for the system with a surface dependent flux (fig. 4.9) deviate even further from the original system. But again the exponents for different interaction ranges show a similar trend. This trend now also shows up for small I, at least for the system with a smaller substrate surface.
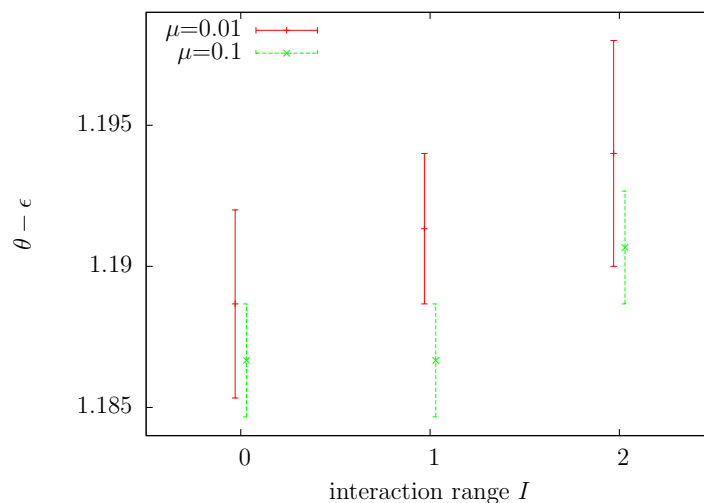
Figure 4.9.: Scaling exponent $\theta - \epsilon$ obtained for different constant values of I and by fitting the slope to data averaged over 20 simulations of a system with homogeneous flux onto the total surface. The fitting range for all graphs is $1e4 < \tau < 1e6$.

We find, that our results do not find Blackmans prediction of $\theta - \tau = 1.17$. They are not only relatively far away from 1.17 but they are also directly dependent on the micro-dynamics of the system.

The calculated values of z' (see tab. A.1 to A.3) are now used to rescale the droplet size distribution.

---

[2]However, a clear linear dependence between ϵ and I is unlikeable because ϵ has to be larger than 0.

5. Scaling of the size distribution

5.1. Different interaction mechanisms

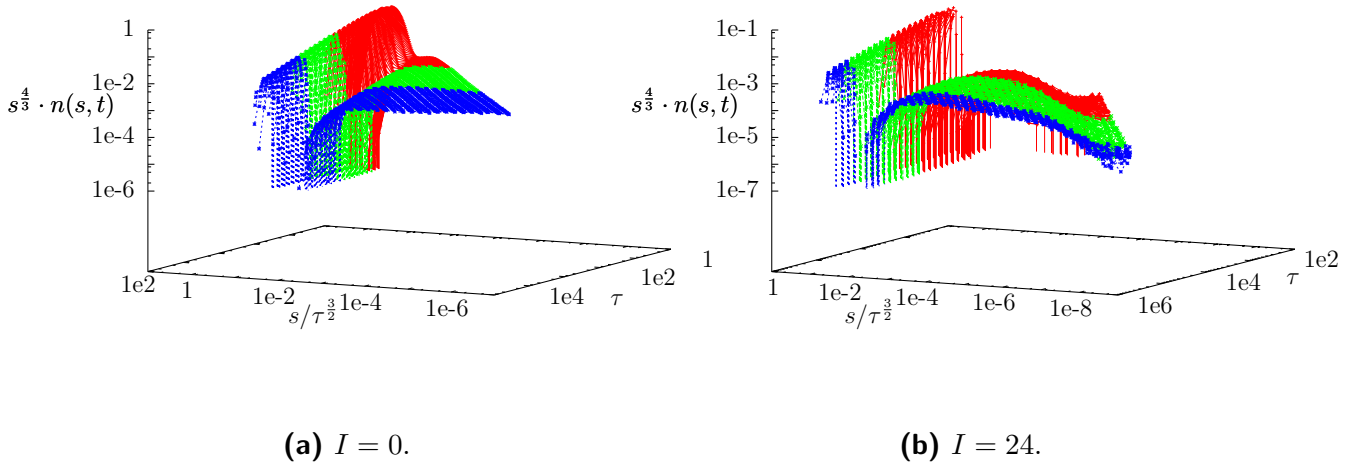

(a) $I = 0$.

(b) $I = 24$.

Figure 5.1.: Evolution of the droplet size distribution over time for two different interaction ranges.

Figure 5.1(a) shows, how the self-similar distribution develops over time, and that it stays more or less constant after a certain amount of time. Also the origin of the 'bump' is shown pretty strikingly. It originates at the very beginning of the evolution and therefore seems to reflect the starting distribution of droplets when the first merging events occur in regime 2. Apparently the influence of this build up of the distribution does not decline over time. In contrast to that, fig. 5.1(b) shows the effect on the evolution of an increased interaction range: The system needs much longer to develop its characteristic droplet distribution, and there are very pronounced new features for smaller droplets for which the simple scaling approach of eq. 2.3 does not account.

Those tails are presented in more detail in fig. 5.2(a). The data for these plots was generated in the same way as for p and n but additionally averaged over half a decade in time ($\tau \in [5 \cdot 10^5, 1 \cdot 10^6]$) since in the asymptotic regime changes in the size distribution mainly occur due to fluctuations.

We observe that for higher values of I the deviations of the small droplets from the

5. Scaling of the size distribution

(a) Scaled using θ.

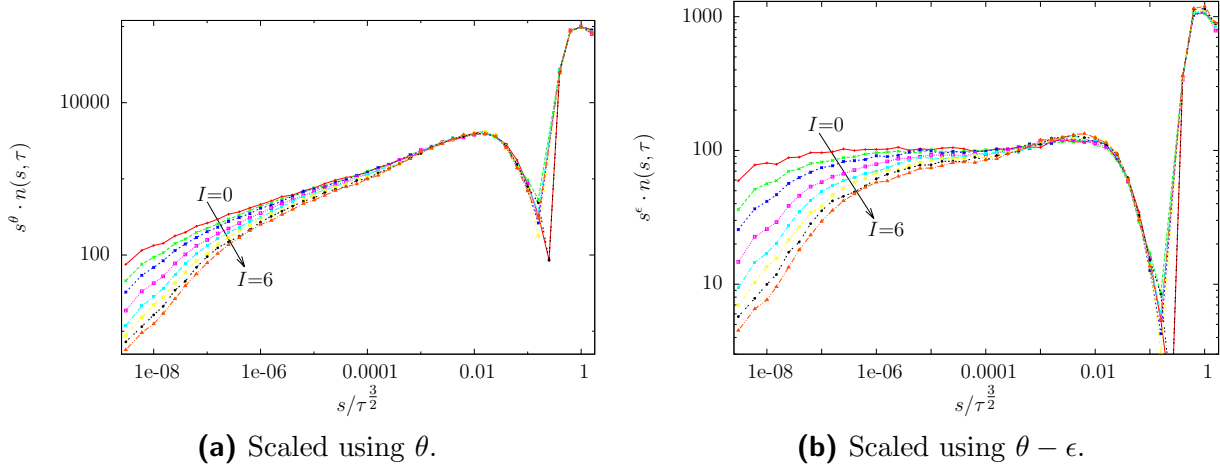**(b)** Scaled using $\theta - \epsilon$.

Figure 5.2.: Influence of different constant interaction ranges I onto the size distribution of droplets. On the right side it is rescaled using the scaling exponent ϵ determined via the porosity.

power-law behaviour grow stronger. Reconsidering eq. 2.12 states an inverse proportionality between $\hat{g}$ and the growth rate $\dot{s}$. This way we find, that by increasing the interaction range the growth rate of the smaller droplets in the system is increased although the growth rate of the large droplets remains unchanged. Eq. 2.13 explains this behaviour: For small droplet also the interaction range has to be taken into account for $\dot{s}$; for larger droplets this correction becomes more and more negligible just as the s_0-term.
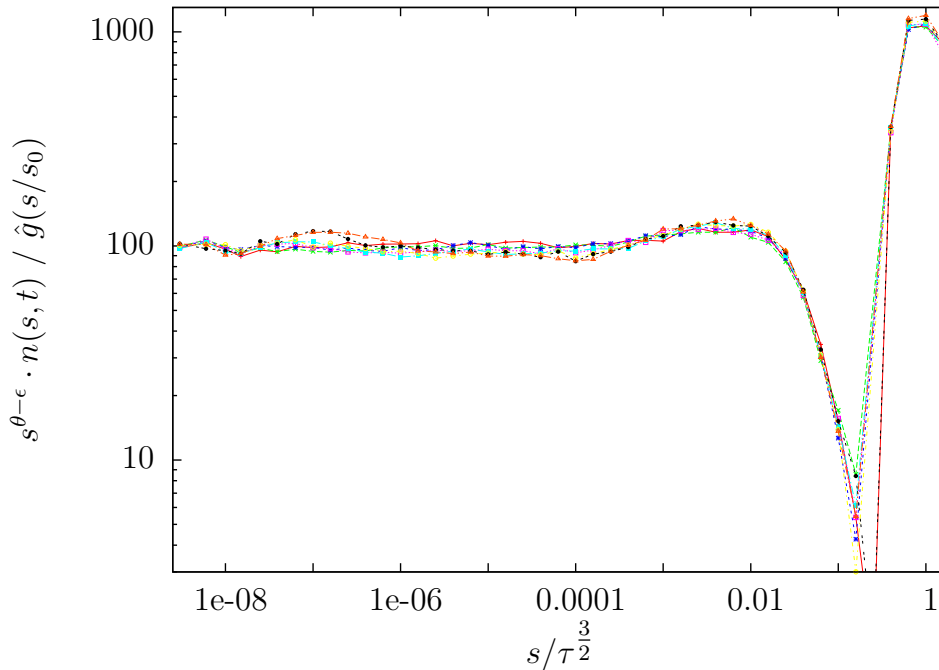

Figure 5.3.: Using the cut-off function $\hat{g}$ to rescale the droplet size distribution for a system with different constant values of I. The size of the system is 10^5.

In fig. 5.2(b) the size distribution is rescaled with ϵ, determined from the porosity (for the exact values see tab. A.1). Thereby the deviations of the small droplets are even more pronounced. And also another feature of the large size cut-off function $\hat{f}$ appears. It is not only accounting for the dip and the bump in the distribution of large sized droplet (see fig. 6.1) but also for a second, lower bump for the droplets slightly smaller than the size the dip appears for. So the actual scaling regime spans only over one to three decades of the size distribution, depending on I.

When we fit the data for the tails with the function for $\hat{g}$ given in eq. 2.14 and also use our results on z' obtained in sec. 4, we can plot the cut-off function $\hat{f} = n \cdot s^{\theta-\epsilon}/\hat{g}$. For this function we obtain a perfect data collapse as demonstrated in fig. 5.3. The fitted values for a and b are given in tab. A.4, $\hat{f}_0$ is the same for all different values of I which allows the assumption, that the systems micro-dynamics have no impact on the large scale cut-off $\hat{f}(s/S)$.

Considering now the triple merge system (see fig. 5.4(a)) we observe a oscillatory behaviour for the small droplets. When rescaled with ϵ a qualitative change in the growth rate for small droplets of different size becomes visible (fig. 5.4(b)). Hence the tail of the distribution is not directly describable by eq. 2.14.

(a) Scaled using θ.　　　　**(b)** Scaled using $\theta - \epsilon$.
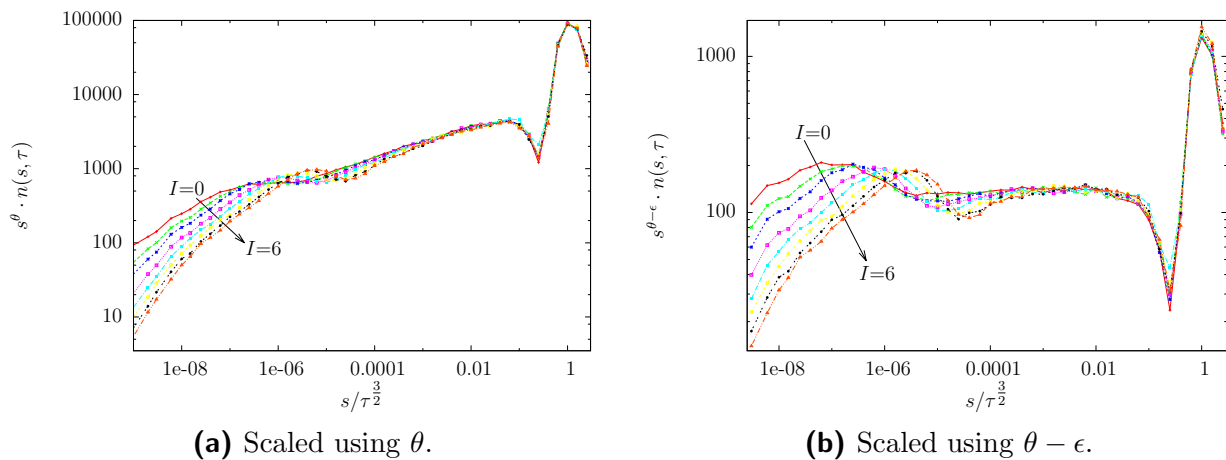
Figure 5.4.: Influence of different constant interaction ranges I onto the size distribution of droplets for a system with the possibility of triple merging events. The size of the system is 10^5.

5.2. Surface dependent flux

For the system with the surface dependent flux we observe a distribution very similar to the original system. One interesting difference occurs when rescaled with ϵ (fig. 5.5(b)): The *second bump* observed in the binary merging system (see fig. 5.2) does not occur here. Again the influence of different values of I are smaller for smaller values of μ. And a collapse of

5. Scaling of the size distribution

(a) Scaled using θ.
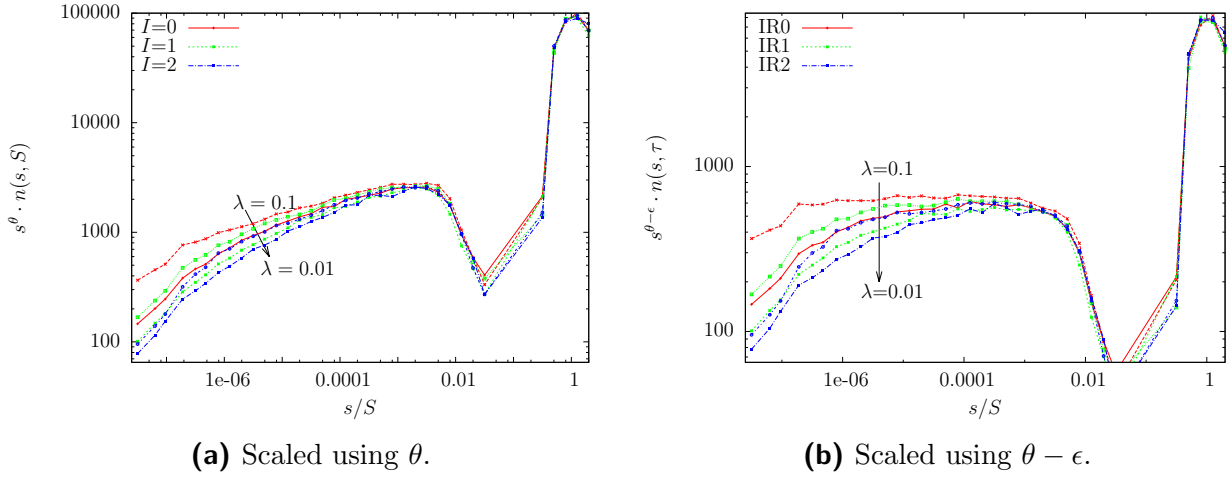
(b) Scaled using $\theta - \epsilon$.

Figure 5.5.: Scaling of the droplet size distribution for different surface depending fluxes. On the right side it is rescaled using the scaling exponent ϵ determined via the porosity.

the data is achieved by fitting eq. 2.14 to the tails and replotting the size distribution using the fitted functions (fig. 5.6). The only new feature is, that here $\hat{f}_0$ is not the same for all different values of I and μ. Instead $\hat{f}_0 \in [545, 650]$.

Figure 5.6.: Using the cut-off function $\hat{g}$ to rescale the droplet size distribution for a system with different constant values of I and a flux which is homogeneous on the total surface of the system. The linear size of the system is 10^5.

6. Conclusion & Outlook

In the present work we showed, that the classical theories describing droplet growth processes for breath figures of droplets on a two dimensional substrate also describe the growth of three dimensional droplets on a one dimensional substrate. In the figure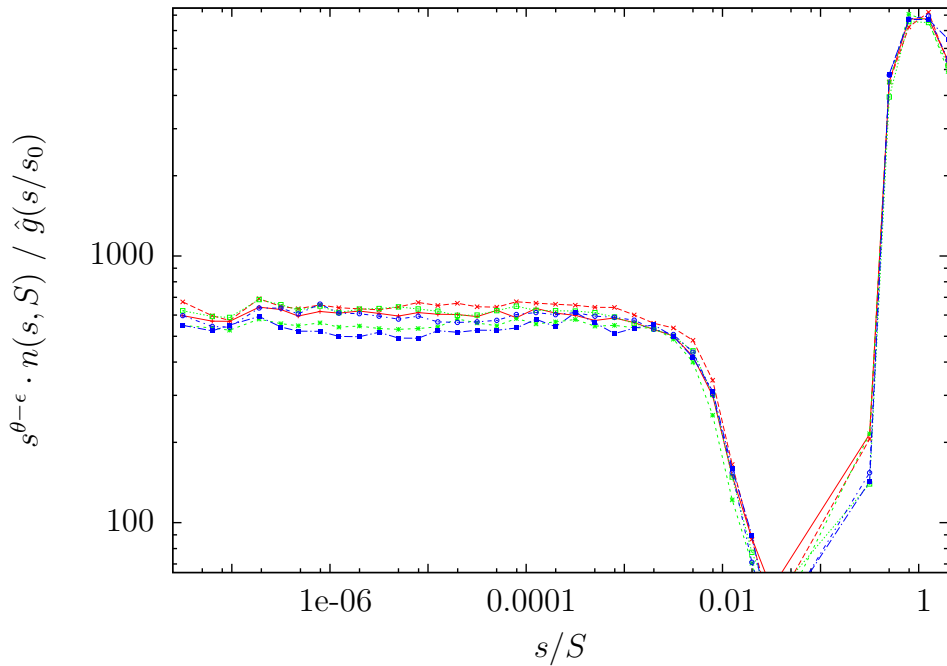s 4.1 to 4.7 we identified three growth regimes in the time evolution of the considered systems: adding droplets to an empty surface, the evolution of a mono-disperse distribution, and the emergence and evolution of a self-similar droplet size distribution. For different interaction mechanisms our simulation data verified the predicted data collapse for constant and radius-dependent interaction ranges (fig. 4.2). It also led to a non-trivial shift in the magnitude of the main observable porosity and the number of droplets (fig. 4.3). This effect becomes particularly visible when allowing the droplets to merge with both neighbours at the same time (fig. 4.4).

The different micro-dynamics enter into the scaling description for the droplet size distribution. The distribution is divided into three parts (see figures 5.2 to 5.6):

1. The distribution of **large droplets** is given by the function $\hat{f}(s/S)$. It involves a *bump* with large droplets, separated by a *gap* from a broad tail describing intermediate-sized droplets. We found that the micro-dynamics have no impact on the growth of the largest droplets in the systems. Hence the scaling function $\hat{f}$ is independent of I. However, there still are deviations for the two analyzed types of flux: For homogeneous flux onto the system surface the gap is much broader than for the homogeneous flux onto the one dimensional substrate (fig. 6.1). So although the surface flux system has the same asymptotic growth law for large droplets it still has an effect on the distribution of large droplets.

2. The behaviour of the **small droplets** is completely different to the large ones. A change of I strongly affects their growth rate. We provided a theoretical function for the tail of the distribution that captures all data for binary collisions with both types of volume flux. Furthermore we showed for the surface dependent flux that the diameter of the string causes notable changes in the tails, although it did not influence the larger droplets. A very surprising result we obtained for systems with triple merging. Even though we clearly distinguished a scaling regime for $\frac{s}{S} \in [1e - 4 : 1e - 1]$, we found an oscillatory behaviour for the growth of the smallest droplets. the function $\hat{g}$ becomes some new, non-trivial function for this case.
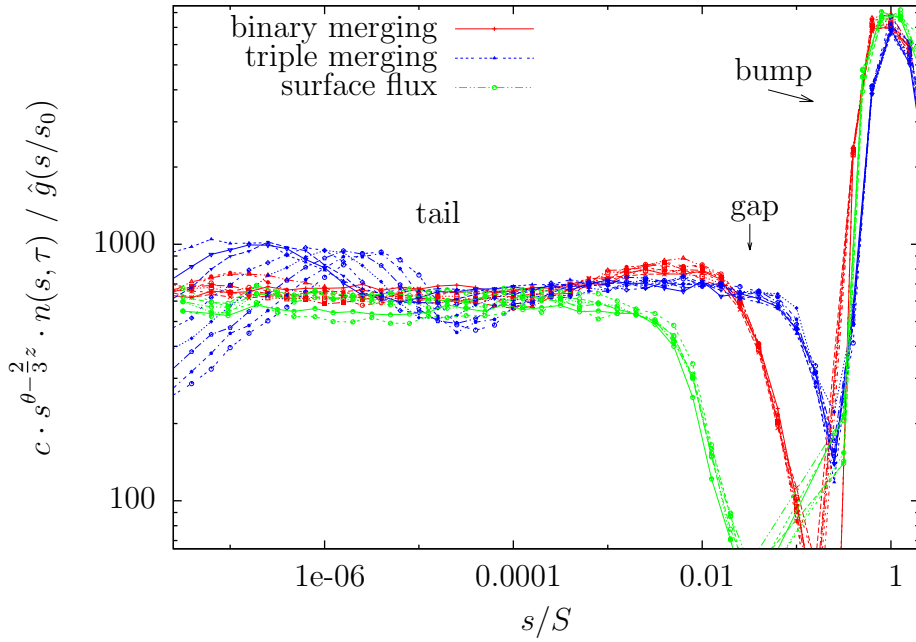
Figure 6.1.: Comparison of the distribution of large droplets for the three types of dynamics. The distribution for binary merging was additionally rescaled with $c = 6.6$ and the distribution for triple merging was rescaled with $c = 5$. In the latter case the tails could not be removed (we used here $\hat{g}(\frac{s}{s_0} = 1)$) due to lack of a theoretical model.

3. The size distribution of **medium sized droplets** follows to a very good approximation a power law involving a non-trivial scaling exponent z'. We showed that the fractal packings ansatz, assuming a fractal dimension $d_f = \frac{2}{3} z'$, is fitting the data for one dimensional substrates. This result further substantiates the finding of [9], that the derivation of Blackman and Brochard [11] for z' must be based on some false or over-simplified assumptions. In contrast to their prediction, that the scaling exponent z' is just depending on the dimension of the droplets and the substrate, we showed, that the microscopic dynamics of the droplet interaction also has to be included in a comprehensive model. Instead of the predicted constant value of $z' = 0.25$, we observe values for z' in a wide range between 0.23 and 0.33 for flux proportional to the thread length, and z' in the quite different range 0.19 to 0.22 for surface dependent flux. All analyzed systems show similar dependences between z' and the droplets interaction range I. Especially for $1 < I \le 6$ a linear trend was observed (see fig. 4.8).

In summary we showed, that the micro-dynamics have a non-negligible influence onto the droplet growth laws and the droplet size distribution. There, naturally, remain many open questions.

One topic rather slightly touched in this work is the specific form of the cut-off function $\hat{f}$ for large droplets. We saw that different interaction rules have a great impact on the porosity and the droplet number density for $\tau \approx 1$ (fig. 4.3 to 4.7). Since this is the growth regime where the distribution of large droplets evolves, deeper understanding of this transition should provide a method for deriving the specific form for $\hat{f}$.

Another aspect that remains open to investigation is the explicit connection between ϵ and I. Although we observed a somehow linear dependence it is obvious that this can only be a low order approximation since ϵ cannot become less than zero and we also saw some different behaviour for small values of I.

Finally, the experiment presented in sec. 1.2.2 should be mentioned. It would be desirable to use this experiment to check in how far the different systems discussed in this work give knowledge about a real system. Especially for investigating the influence of the thickness of the string this experiment should fit well.

A. Appendix

A.1. Values of fitted parameters

The following tables present all values that were obtained by fitting the data and that were later used to rescale the droplet size distribution. The fits were performed with gnuplot, which uses the nonlinear least-squares Levenberg-Marquadt algorithm.

I	z'	$\sigma_{z'}$	$\theta - \epsilon$	$\sigma_{\theta-\epsilon}$
0.0	0.3281	0.0009	1.1146	0.0006
0.5	0.3288	0.0006	1.1141	0.0004
1.0	0.3277	0.0006	1.1149	0.0004
2.0	0.3268	0.0005	1.1155	0.0004
3.0	0.3254	0.0005	1.1164	0.0004
4.0	0.3233	0.0005	1.1178	0.0004
5.0	0.3218	0.0005	1.1188	0.0004
6.0	0.3198	0.0006	1.1201	0.0004
8.0	0.3176	0.0007	1.1216	0.0005
12.0	0.3121	0.0007	1.1253	0.0005
16.0	0.3086	0.0006	1.1276	0.0004
24.0	0.3029	0.0007	1.1314	0.0005

Table A.1.: Exponent z' for system with different constant I and flux proportional to the substrates length determined via fit to the porosity over time interval [1e4:1e6].

I	z'	$\sigma_{z'}$	$\theta - \epsilon$	$\sigma_{\theta-\epsilon}$
0.0	0.3058	0.0008	1.1295	0.0006
0.5	0.3055	0.0007	1.1297	0.0005
1.0	0.3043	0.0006	1.1305	0.0004
2.0	0.3029	0.0006	1.1314	0.0004
3.0	0.3009	0.0006	1.1327	0.0004
4.0	0.2991	0.0006	1.1339	0.0004
5.0	0.2973	0.0006	1.1351	0.0004
6.0	0.2952	0.0007	1.1365	0.0005

Table A.2.: Exponent z' for system with different constant I, the flux proportional to the substrates length and the possibility of three merging events at one time step determined via fit to the porosity over time interval [1e4:1e7].

I	δ	z'	$\sigma_{z'}$	$\theta - \epsilon$	$\sigma_{\theta-\epsilon}$
0	0.01	0.217	0.005	1.189	0.004
	0.1	0.22	0.003	1.187	0.002
1	0.01	0.213	0.004	1.191	0.003
	0.1	0.22	0.003	1.187	0.002
2	0.01	0.209	0.005	1.194	0.004
	0.1	0.214	0.004	1.191	0.003

Table A.3.: Exponent z' for system with different constant I and surface dependent flux, with different weights for the surface of the string, determined via fit to the porosity over time interval [1e4:1e6].

I	$\hat{f}_0$	a	σ_a	b	σ_b
0.0	100	$2.4{\cdot}10^{-5}$	$1.8{\cdot}10^{-5}$	0.98	0.08
0.5	100	0.0012	0.0004	0.7	0.04
1.0	100	0.0044	0.0008	0.623	0.017
2.0	100	0.011	0.003	0.6	0.02
3.0	100	0.017	0.003	0.606	0.014
4.0	100	0.024	0.002	0.608	0.007
5.0	100	0.046	0.007	0.567	0.015
6.0	100	0.057	0.009	0.57	0.02

Table A.4.: Numerically determined parameters of $\hat{g}$ for system with different constant I and flux proportional to the substrates length determined via fit to the rescaled droplet size distribution in the interval $\frac{s}{S} \in [1e\text{-}9 : 8e\text{-}5]$.

I	μ	$\hat{f}_0$	a	σ_a	b	σ_b
0	0.01	590	$2.7{\cdot}10^{-4}$	$1{\cdot}10^{-4}$	0.54	0.02
	0.1	650	$4{\cdot}10^{-7}$	$6{\cdot}10^{-7}$	0.85	0.11
1	0.01	545	$1.6{\cdot}10^{-4}$	$6{\cdot}10^{-5}$	0.565	0.012
	0.1	615	$5{\cdot}10^{-5}$	$3{\cdot}10^{-5}$	0.63	0.03
2	0.01	545	$2.4{\cdot}10^{-4}$	$6{\cdot}10^{-5}$	0.587	0.015
	0.1	580	$5{\cdot}10^{-5}$	$3{\cdot}10^{-5}$	0.67	0.03

Table A.5.: Numerically determined parameters of $\hat{g}$ for system with different constant I determined and a surface dependent flux via fit to the rescaled droplet size distribution in the interval $\frac{s}{S} \in [1e\text{-}9 : 8e\text{-}5]$.

A.2. Shape of droplets on strings

The following derivation has been adopted from notes by [14].

To derive the contact angle that droplets form on a string we firstly consider its surface area A and volume V depending on its contour, assuming it to have rotational symmetry around the string:

$$A_L[f(x)] = 2\pi \int_{-L}^{L} dx\, f(x) \cdot \sqrt{1 + [f'(x)]^2},$$

$$V_L[f(x)] = \pi \int_{-L}^{L} dx\, f^2(x).$$

Here $f(x)$ denotes the droplets' shape and $2L$ its length on the string. Using eq. 1.1, its energy E adds up to

$$E = \int_{-L}^{L} dx\, \left[\gamma_{LG}\left(2\pi\, f(x) \cdot \sqrt{1 + f'^2(x)}\right) - \gamma_{SG} + \gamma_{SL} + \varsigma \cdot \pi \cdot f^2(x)\right] =: \int_{-L}^{L} dx\, \varepsilon(x)$$

where ς denotes the chemical potential. Using the Lagrangian $\frac{\partial \varepsilon}{\partial f} = \frac{d}{dx}\frac{\partial \varepsilon}{\partial f'}$ one finds:

$$\gamma_{LG} \cdot \sqrt{1 + f'^2} + \varsigma \cdot f = \frac{d}{dx}\left[\frac{\gamma_{LG} \cdot f \cdot f'}{\sqrt{1 + f'^2}}\right].$$

Rewriting $x \to \frac{x}{L}$, $f \to \frac{f}{L}$ and defining $M = \frac{\varepsilon \cdot L}{\gamma_{LG}}$ this leads to

$$\sqrt{1 + f'} + M \cdot f = \frac{d}{dx}\left[\frac{f \cdot f'}{\sqrt{1 + f'}}\right]. \tag{A.1}$$

For a spherical droplet the form $f(x) = \sqrt{1 - x^2}$ leads to $M = -2$. Instead considering an ellipsoid we find

$$f(x, \alpha \qquad \Rightarrow \qquad M = -\frac{1}{\alpha} - 1. \tag{A.2}$$

Repeating the steps for calculating the Lagrangian including α leads to

$$\frac{\varepsilon(L)}{\gamma_{LG}} = \frac{3\,V_L}{\alpha \cdot L} + \left(\frac{\gamma_{SL} - \gamma_{SG}}{\gamma_{LG}}\right) \cdot L = -\frac{3\varsigma V}{\gamma_{LG}} - \frac{3V}{L} - \frac{L}{\cos\theta}.$$

Considering now a string with a finite thickness ρ reduces both limits of the integration by

A. Appendix

$\frac{\rho}{L}$. Again repeating the steps we find

$$
\begin{aligned}
\frac{\varepsilon_L(\rho)}{\gamma_{LG}} &= A_{(\rho)} + \frac{\gamma_{SL} - \gamma_{SG}}{\gamma_{LG}} \cdot 2\pi\rho \cdot L \\
&= \frac{2 \cdot V(\rho)}{\alpha \cdot L \cdot \left(1 - \frac{1}{3} \cdot (1 - \frac{\rho}{L})^2\right)} - \frac{2\pi\rho\,L}{\cos\theta} \\
&= -\frac{2\varsigma\,V}{\gamma_{LG} \cdot \left[1 - \frac{1}{3} \cdot (1 - \frac{\rho}{L})^2\right]} - \frac{2\,V}{1 - \frac{1}{3} \cdot (1 - \frac{\rho}{L})^2} \cdot \frac{1}{L} - \frac{2\pi\rho}{\cos\theta} \cdot L.
\end{aligned}
$$

When taking the limit $\rho \to 0$ we get:

$$
\begin{aligned}
\frac{d\varepsilon_L(\rho)}{dL} = 0 \quad &\Leftrightarrow \quad \frac{2\,V}{L^2} \simeq \frac{2\pi\rho}{\cos\theta} \qquad\qquad (\alpha \simeq 2,\ \rho \simeq 0) \\
&\Leftrightarrow \quad \frac{2\pi\rho}{\cos\theta} \simeq \frac{3 \cdot \frac{4\pi}{3}L^3}{L^2} = 4\pi\,L \quad \Leftrightarrow \quad \frac{\rho}{2\,L} = \cos\theta = \frac{\pi}{2} - \theta \\
&\Leftrightarrow \quad \theta \simeq \frac{\pi}{2} - \frac{\rho}{2\,L}.
\end{aligned}
$$

Bibliography

[1] Rayleigh, *Breath figures*, Nature **86(2258)**, 416 (1911)

[2] G. D. Bansal, S. Khandekar, K. Muralidhar, *Measurement of heat transfer during drop-wise condensation of water on polyethylene*, Nanoscale and Microscale Thermophysical Engineering **13(3)**, 184 (2009)

[3] D. Beysens, *Dew nucleation and growth*, Comptes Rendus Physique **7(9)**, 1082 (2006)

[4] O. Klemm, et al., *Fog as a fresh-water resource: Overview and perspectives*, AMBIO **41(3)**, 221 (2012)

[5] R. S. Schemenauer, P. I. Joe, *The collection efficiency of a massive fog collector*, Atmospheric Research **24(1–4)**, 53 (1989)

[6] J. L. Viovy, D. Beysens, C. M. Knobler, *Scaling description for the growth of condensation patterns on surfaces*, Physical Review A **37(12)**, 4965 (1988)

[7] D. Beysens, C. Knobler, *Growth of breath figures*, Physical review letters **57(12)**, 1433 (1986)

[8] T. Lapp, *Evolution of droplet distributions in hydrodynamic systems*, Ph.D. thesis, Georg-August-University Göttingen (2011)

[9] J. Blaschke, T. Lapp, B. Hof, J. Vollmer, *Breath figures: Nucleation, growth, coalescence, and the size distribution of droplets*, arXiv (2012)

[10] F. Family, P. Meakin, *Kinetics of droplet growth processes: Simulations, theory, and experiments*, Physical Review A **40(7)**, 3836 (1989)

[11] J. A. Blackman, S. Brochard, *Polydispersity exponent in homogeneous droplet growth*, Phys. Rev. Lett. **84**, 4409 (2000)

[12] D. Fritter, C. M. Knobler, D. A. Beysens, *Experiments and simulation of the growth of droplets on a surface (breath figures)*, Physical Review A **43(6)**, 2858 (1991)

[13] K. Graf, M. Kappl, et al., *Physics and chemistry of interfaces*, John Wiley & Sons (2006)

Bibliography

[14] J. Vollmer, *Notes and Dicsussions* (2013)

[15] T. Rogers, K. Elder, R. C. Desai, *Droplet growth and coarsening during heterogeneous vapor condensation*, Physical Review A **38(10)**, 5303 (1988)

[16] J. Rose, L. Glicksman, *Dropwise condensation—the distribution of drop sizes*, International Journal of Heat and Mass Transfer **16(2)**, 411 (1973)

[17] H. Tanaka, *Measurements of drop-size distributions during transient dropwise condensation*, Journal of Heat Transfer **97(3)**, 341 (1975)

[18] F. Family, P. Meakin, *Scaling of the droplet-size distribution in vapor-deposited thin films*, Physical review letters **61(4)**, 428 (1988)

Acknowledgments

Firstly, I would like to thank my supervisor Jürgen Vollmer for all his support on this project. All the ideas and inspiring discussions he contributed have been very helpful while creating this thesis. He always had a sympathetic ear, irrespective of the time of day or his own workload.

Furthermore I would like to thank all the members of Jürgens and Marcos group for all help and ideas concerning my research and also for creating such a pleasant and inspiring environment. In particular I want to thank Johannes, Laura, Martin and Bernhard for always having profound comments and suggestions for my work and everything else, and especially Artur for all help with irritating IT problems.

All of them helped me through that likewise challenging and motivating first hurdle of my academic career.

Also I would like to thank Eleni Katifori for her commitment as a referee at such a short notice.

Erklärung nach §13(8) der Prüfungsordnung für den Bachelor-Studiengang Physik und den Master-Studiengang Physik an der Universität Göttingen:

Hiermit erkläre ich, dass ich diese Abschlussarbeit selbständig verfasst habe, keine anderen als die angegebenen Quellen und Hilfsmittel benutzt habe und alle Stellen, die wörtlich oder sinngemäß aus veröffentlichten Schriften entnommen wurden, als solche kenntlich gemacht habe.

Darüberhinaus erkläre ich, dass diese Abschlussarbeit nicht, auch nicht auszugsweise, im Rahmen einer nichtbestandenen Prüfung an dieser oder einer anderen Hochschule eingereicht wurde.

Göttingen, den August 22, 2013

(Gunnar Klös)